

All entangled states can be certified by a violation of noncontextuality inequalities

Yujie Zhang,^{1, 2, *} Jonah Spodek,¹ David Schmid,² Carter Reid,¹ Liam J. Morrison,^{1, 3} Thomas Jennewein,^{1, 4} Kevin J. Resch,¹ and Robert W. Spekkens²

¹ Institute for Quantum Computing and Department of Physics & Astronomy,
University of Waterloo, 200 University Ave W, Waterloo, Ontario, N2L 3G1, Canada

² Perimeter Institute for Theoretical Physics, 31 Caroline Street North, Waterloo, Ontario Canada N2L 2Y5

³ Department of Physics and Atmospheric Science,
Dalhousie University, Halifax, Nova Scotia, Canada B3H 3J5

⁴ Department of Physics, Simon Fraser University,
8888 University Dr W, Burnaby, BC V5A 1S6, Canada

(Dated: July 25, 2025)

By combining the assumption of Bell locality with that of generalized noncontextuality, we define different classes of noncontextuality inequalities for correlations in a bipartite Bell scenario. These classes are distinguished by which operational identities are enforced, where certain natural subsets form a hierarchy and provide a new way to understand and classify different forms of quantum correlations. Specifically, we show that violations of inequalities at different levels of this hierarchy can serve as witnesses to determine whether a bipartite quantum state exhibits entanglement, steering, or nonlocality, thereby giving a systematic and unified method for certifying these distinct bipartite quantum resources. To illustrate the power of this approach, we demonstrate the violation of one such inequality in an experiment with polarization-entangled photons. This experimental implementation enables us to certify entanglement in certain two-qubit isotropic states for which certification by Bell or steering inequalities is known to be impossible. Our entanglement certification scheme is the first to combine all of the following desirable features: it requires no prior characterization of the measurements, it delivers a verdict based on quantities that are independent of the tomographic gauge freedom, and it is able to certify *any* entangled state without requiring any auxiliary entangled sources.

I. INTRODUCTION

Distinguishing whether a given operational behavior is classically explainable or genuinely quantum is a central problem in the foundations of quantum mechanics. As is well known, certain quantum experiments exhibit correlations that cannot be explained within a classical model that respects the natural causal structure of the experiment. For example, there is no local (i.e., common-cause) explanation for quantum correlations in a Bell scenario [1, 2]. In addition to Bell nonlocality [3], other types of correlations that arise naturally in this scenario include entanglement [4] and steerable correlations [5].

These concepts play a central role in quantum information science and have been extensively studied [6–8], yet there is no consensus on how to best understand the relationship between them [9, 10]. While all pure entangled states exhibit nonlocality [11, 12], for mixed states the connection between entanglement and nonlocality is less clear [6, 13]. As a consequence, Bell inequalities [14], which serve as device-independent tests of nonlocality, cannot detect all entangled states in a standard Bell scenario, and alternative approaches such as quantum state tomography, entanglement witnesses, and measurement device-independent tests have been developed to verify entanglement in practical settings [15–17].

We suggest, alternatively, that nonclassicality should be understood as the failure of operational statistics to be realizable by a noncontextual ontological model (NCOM) [18], a property that we shall refer to as *NCOM-nonrealizability*.¹ A noncontextual ontological model imposes constraints on the representation of each component of a quantum circuit based on the specific operational identities that they satisfy (where an operational identity is simply any equality holding among the different possibilities for a component in the circuit [21]). This approach generalizes the notion of Kochen–Specker noncontextuality from projective measurements to arbitrary quantum processes, and generalizes the notion of negativity of the Wigner function to arbitrary quasiprobabilistic representations [22, 23]. NCOM-nonrealizability also coincides with the failure of the natural notion of classical-explainability in generalized probabilistic theories [23–25]. Recent efforts have made some connections between NCOM-nonrealizability and various forms of bipartite states [30–32]. However, these studies have focused on comparing bipartite quantum resources to NCOM-nonrealizability in certain prepare-measure sce-

¹ Note that throughout this work, we use the term *noncontextual* to refer to the notion of generalized noncontextuality defined in Ref. [18] rather than the Kochen–Specker notion [19, 20]. We use the term *NCOM-nonrealizable* in preference to *contextual* to emphasize that in the face of a no-go result, one has the option to abandon the framework of ontological models, rather than the principle of noncontextuality.

* yujie4physics@gmail.com

Entanglement Certification	Features				
	No prior characterization of measurements	Independent of tomographic gauge	Able to certify any entangled state	No additional entangled sources	No assumption of tomographic completeness
Separability test with quantum state tomography	✗	✓	✓	✓	✗
Entanglement witness [15]	✗	✓	✓	✓	✓
Separability test with GPT/gate-set tomography [26, 27]	✓	✗	✓	✓	✗
Bell inequality test in Bell scenario [3, 28]	✓	✓	✗	✓	✓
Inequality test in non-Bell network scenario [29]	✓	✓	✓	✗	✓
Noncontextuality inequality test (Our approach)	✓	✓	✓	✓	✗

TABLE I. A summary of the advantages of various methods of entanglement certification.

narios where the set of preparations are induced by the bipartite state through steering. As we will show, examining NCOM-nonrealizability within a bipartite scenario reveals more direct connections to the different classes of bipartite quantum resources.

We introduce the notion of NCOM-realizability for operational statistics within a bipartite scenario where we denote the two parties as Alice and Bob, who can perform local measurements. We demonstrate that different classes of bipartite quantum states function as resources for establishing NCOM-nonrealizability, depending on the specific set of operational identities taken into account. More precisely, we explore four distinct classes of operational identities: (i) the union of those that hold among Alice's measurements and those that hold among Bob's measurements, (ii) only those that hold among Bob's measurements, (iii) only those that hold among Alice's measurements, and (iv) the trivial set. We prove that the quantum states that are necessarily NCOM-nonrealizable relative to these classes correspond, respectively, to the entangled states, the unsteerable states from Alice to Bob, the unsteerable states from Bob to Alice, and the nonlocal states.

Additionally, our framework provides novel tools for witnessing membership in these classes through distinct sets of noncontextuality (NC) inequalities. The inequalities derived from considering the class (i), i.e., the union of the set of all operational identities associated to each party are particularly noteworthy, as they are capable of certifying the entanglement of *any* entangled state, including those that are local and unsteerable. This significantly extends the reach of entanglement certification beyond the limitations of standard Bell and steering inequalities. As a concrete illustration, we derive several such inequalities and experimentally demonstrate the violation of one of these, thereby certifying the entanglement of a class of two-qubit isotropic states that are both local and unsteerable, and which consequently cannot be certified using conventional Bell or steering inequalities.

Finally, we also compare the merits of our technique to those of other existing entanglement certification techniques, such as quantum state tomography, entanglement witnesses [15], gate set tomography [27], GPT tomogra-

phy [26], Bell inequality tests [3], and other causal compatibility tests within more complex causal networks [33]. As summarized in Table I, our approach achieves a set of features that is not achieved by any of these pre-existing methods.

II. THEORETICAL RESULTS

A. Noncontextual Ontological Models

The notion of NCOM-realizability provides a rigorous framework for assessing the classical explainability of an operational theory or a set of statistics (i.e., experimental data) [18]. In the simplest prepare-measure scenario, one seeks an ontological model that reproduces the statistics of a quantum circuit where a set of quantum states $\mathbf{P} := \{\rho_x\}_x$ represents the set of *preparations* and a set of POVMs $\mathbf{M} := \{\{M_{b|y}\}_b\}_y$ represents the set of *measurements*. (See Fig. 1(a).) Such a quantum circuit is *classically explainable* if the statistics it predicts can be realized by a generalized-noncontextual ontological model.² This is the case if it is possible to write

$$p(b|xy) := \text{Tr}[\rho_x M_{b|y}] = \sum_{\lambda} p(b|y, \lambda)p(\lambda|x), \quad (1)$$

where $p(\lambda|x)$ denotes a probability distribution over ontic states $\lambda \in \Lambda$ given preparation x , and $p(b|y, \lambda)$ is the response function specifying the probability of outcome b of measurement y given that the ontic state was λ , and where the principle of generalized noncontextuality implies that $p(\lambda|x)$ must be a linear function of the quantum state ρ_x , and $p(b|y, \lambda)$ must be a linear function of the

² Strictly speaking, the notion of noncontextuality can only be applied to ontological models of theories that are not quotiented relative to operational equivalences, whereas in this work we treat quantum theory as a theory wherein this quotienting procedure has been applied [23, 34]. Refs. [23, 24] introduce more precise terminology, but we eschew it here for the sake of maintaining familiar terminology.

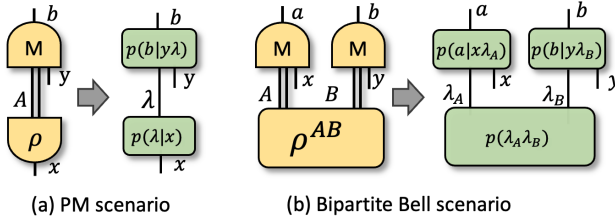


FIG. 1. (a) a unipartite prepare-measure (PM) circuit; (b) a bipartite prepare-measure circuit, i.e., a *bipartite Bell scenario* involving two parties labeled Alice (A) and Bob (B). A classical explanation for a given quantum circuit is given by a linear and diagram-preserving map from the quantum representation to an ontological representation; i.e., to a circuit wherein systems are classical variables and transformations are (sub)stochastic maps on these variables.

effect $M_{b|y}$. A given theory or experiment is then said to be NCOM-nonrealizable if and only if no such representation is possible. NCOM-nonrealizability is the notion of nonclassicality we use in this work.

Although the question of NCOM-realizability has usually been studied only in the prepare-measure scenario just discussed, it is equally applicable to circuits that involve more complex structure and more quantum processes [23, 35]. In this letter, we focus on the particular circuit depicted in Fig. 1(b), consisting of a bipartite quantum state ρ^{AB} and two sets of local measurements, on Alice (A) and Bob (B), denoted $\mathbf{N} := \{\{N_{a|x}\}_a\}_x$ and $\mathbf{M} := \{\{M_{b|y}\}_b\}_y$, as shown in Fig. 1(b). We refer to such a circuit as a *bipartite Bell scenario*, and a specific Bell scenario will be denoted by a $\mathcal{B} := (\mathbf{N}, \mathbf{M}, \rho)$. A multipartite Bell scenario is defined similarly and will be discussed at the end of the paper.

B. Noncontextual ontological models in a Bipartite Bell Scenario

For the bipartite prepare-measure scenario, i.e., the Bell scenario depicted in Fig. 1(b), quantum theory predicts the following operational statistics:

$$p(ab|xy) = \text{Tr}[\rho^{AB} N_{a|x} \otimes M_{b|y}], \quad (2)$$

representing the correlations obtained from performing a local measurement on A with setting x outcome a and a local measurement on B with setting y and outcome b . These operational statistics are classically explainable if this quantum circuit can be mapped to a corresponding ontological model in a linear and diagram-preserving manner that reproduces the observed statistics [23]. We now review the two key structural features that characterize such noncontextual ontological models when specialized to the Bell circuit.

Diagram-preservation (locality) — The ontological representation must preserve the circuit structure. In this representation, a bipartite state is represented by a joint probability distribution $p(\lambda_A \lambda_B)$ over the Cartesian product of the local ontic state spaces, $\lambda_A \times \lambda_B$, and the measurements $\{N_{a|x}\}_a$ and $\{M_{b|y}\}_b$ are represented by sets of response functions $\{p(a|x, \lambda_A)\}_a$ and $\{p(b|y, \lambda_B)\}_b$ respectively. Accordingly, diagram-preservation (locality) implies that the operational statistics must be reproduced as

$$p(ab|xy) = \sum_{\lambda_A \lambda_B} p(\lambda_A \lambda_B) p(a|x, \lambda_A) p(b|y, \lambda_B), \quad (3)$$

Note that this is exactly the standard form of a local hidden variable model for a Bell scenario [3].

Linearity (noncontextuality) — An operational identity satisfied by a set of measurements $\mathbf{N} = \{\{N_{a|x}\}_a\}_x$ has the form $\sum_{a,x} \alpha_{a,x} N_{a|x} = \emptyset$, and is therefore defined by the vector of coefficients $\vec{\alpha} := (\alpha_{a,x})_{a,x}$. Let $\mathcal{O}_{\text{all}}(\mathbf{N})$ represent the set of all vectors associated to operational identities of \mathbf{N} . Let similar definitions hold for any set of measurements, including \mathbf{M} . Explicitly,

$$\mathcal{O}_{\text{all}}(\mathbf{N}) := \{\vec{\alpha} \mid \sum_{a,x} \alpha_{a,x} N_{a|x} = \emptyset\}, \quad (4a)$$

$$\mathcal{O}_{\text{all}}(\mathbf{M}) := \{\vec{\beta} \mid \sum_{b,y} \beta_{b,y} M_{b|y} = \emptyset\}, \quad (4b)$$

For an ontological model that is noncontextual, the set of response functions $\{\{p(a|x, \lambda_A)\}_a\}_x$ representing the set of measurements $\mathbf{N} = \{\{N_{a|x}\}_a\}_x$, must be obtained from the latter by a linear map; similarly for the set of response functions $\{\{p(b|y, \lambda_B)\}_b\}_y$ representing the set of measurements $\mathbf{M} = \{\{M_{b|y}\}_b\}_y$. This implies that these response functions must satisfy the same identities as are satisfied by the effects, that is,

$$\sum_{ax} \alpha_{a,x} p(a|x, \lambda_A) = 0 \quad \forall \vec{\alpha} \in \mathcal{O}_{\text{all}}(\mathbf{N}), \quad (5a)$$

$$\sum_{by} \beta_{b,y} p(b|y, \lambda_B) = 0 \quad \forall \vec{\beta} \in \mathcal{O}_{\text{all}}(\mathbf{M}). \quad (5b)$$

Unlike for a unipartite prepare-measure scenario, there exist non-trivial compositions of processes within a bipartite Bell scenario, namely,

$$\mathbf{N} \circ \rho := \{\{\text{Tr}_A[(N_{a|x} \otimes \mathbb{1}) \rho^{AB}]\}_a\}_x = \{\{\tilde{\rho}_{a|x}^B\}_a\}_x, \quad (6a)$$

$$\mathbf{M} \circ \rho := \{\{\text{Tr}_B[(\mathbb{1} \otimes M_{b|y}) \rho^{AB}]\}_b\}_y = \{\{\tilde{\rho}_{b|y}^A\}_b\}_y. \quad (6b)$$

Here, $\{\{\tilde{\rho}_{a|x}^B\}_a\}_x$ and $\{\{\tilde{\rho}_{b|y}^A\}_b\}_y$ are steering assemblages [36, 37] on party B and A respectively.

An operational identity satisfied by a steering assemblage $\{\{\tilde{\rho}_{a|x}^B\}_a\}_x$ has the form $\sum_{a,x} \alpha_{a,x} \tilde{\rho}_{a|x}^B = \emptyset$, and is therefore defined by the vector of coefficients $\vec{\alpha} := (\alpha_{a,x})_{a,x}$. Let $\mathcal{O}_{\text{all}}(\mathbf{N} \circ \rho)$ represent the set of all vectors

associated to operational identities of $\mathbf{N} \circ \rho$, and similarly for $\mathbf{M} \circ \rho$, that is,

$$\mathcal{O}_{\text{all}}(\mathbf{N} \circ \rho) := \{\vec{\alpha} \mid \sum_{a,x} \alpha_{a,x} \tilde{\rho}_{a|x}^B = 0\}, \quad (7a)$$

$$\mathcal{O}_{\text{all}}(\mathbf{M} \circ \rho) := \{\vec{\beta} \mid \sum_{b,y} \beta_{b,y} \tilde{\rho}_{b|y}^A = 0\}. \quad (7b)$$

The steering assemblage on B , $\{\{\tilde{\rho}_{a|x}^B\}_a\}_x$, is represented in the ontological model by a set of subnormalized distributions, $\{\{\tilde{\rho}(\lambda_B a|x)\}_a\}_x$, where

$$\tilde{\rho}(\lambda_B a|x) := \sum_{\lambda_A} p(a|x\lambda_A) p(\lambda_A \lambda_B), \quad (8)$$

and similarly for the steering assemblage on A . Noncontextuality implies that each of these sets of distributions must be the image of a linear map on the respective steering assemblage, implying the following constraints on the ontological representations of the bipartite state and local measurements:

$$\sum_{ax} \alpha_{a,x} \left[\sum_{\lambda_A} p(a|x\lambda_A) p(\lambda_A \lambda_B) \right] = 0 \quad \forall \vec{\alpha} \in \mathcal{O}_{\text{all}}(\mathbf{N} \circ \rho), \quad (9a)$$

$$\sum_{by} \beta_{b,y} \left[\sum_{\lambda_B} p(b|y\lambda_B) p(\lambda_A \lambda_B) \right] = 0 \quad \forall \vec{\beta} \in \mathcal{O}_{\text{all}}(\mathbf{N} \circ \rho). \quad (9b)$$

For a specific Bell scenario $\mathcal{B} = (\mathbf{N}, \mathbf{M}, \rho)$, the operational statistics $p(ab|xy)$ are said to be NCOM-realizable [35] if they can be realized by a diagram-preserving (and hence local) model, as in Eq. (3), while also respecting the implications of noncontextuality for the full set of operational identities on each of \mathbf{N} , \mathbf{M} , $\mathbf{N} \circ \rho$, and $\mathbf{M} \circ \rho$ (i.e., while respecting Eq. 5 and Eq. 9). We denote the set of all such statistics by \mathcal{NC} .

One can also define various necessary (but in general not sufficient) conditions on operational statistics $p(ab|xy)$ for them to be NCOM-realizable. These conditions arise when one applies the principle of noncontextuality to subsets of the full set of operational identities for one or more of \mathbf{N} , \mathbf{M} , $\mathbf{N} \circ \rho$, and $\mathbf{M} \circ \rho$.

For each of \mathbf{N} , \mathbf{M} , $\mathbf{N} \circ \rho$, and $\mathbf{M} \circ \rho$, we consider a single alternative to the full set of operational identities thereon, namely, what we term the trivial set. For example, the trivial set of operational identities for \mathbf{N} , denoted $\mathcal{O}_{\text{triv}}(\mathbf{N})$, is all and only those that arise from the completeness condition $\sum_a N_{a|x} = \sum_a N_{a|x'} = 1$. These identities are deemed to be trivial because the corresponding ontological identities are automatically satisfied simply by the definition of a set of response functions, i.e., $\sum_a p(a|x\lambda_A) = \sum_a p(a|x'\lambda_A)$. Similarly, the set $\mathcal{O}_{\text{triv}}(\mathbf{N} \circ \rho)$ represents those operational identities that arise from the no-signalling condition $\sum_a \tilde{\rho}_{a|x}^B = \sum_a \tilde{\rho}_{a|x'}^B$, which are trivial because the corresponding ontological identities are automatically satisfied due to the

assumption of diagram-preservation, i.e., $\sum_a \tilde{\rho}(a\lambda_B|x) = \sum_a \tilde{\rho}(a\lambda_B|x')$.

Hence, in a specific Bell scenario $\mathcal{B} = (\mathbf{N}, \mathbf{M}, \rho)$, for each of \mathbf{N} , \mathbf{M} , $\mathbf{N} \circ \rho$, $\mathbf{M} \circ \rho$, we can associate a binary variable that stipulates whether we use \mathcal{O}_{all} or $\mathcal{O}_{\text{triv}}$ for it. That is, letting $i, j, u, v \in \{a, t\}$, where a stands for ‘all’ and t stands for ‘trivial’, one can define

$$\mathcal{O}_{ijuv}(\mathcal{B}) := \mathcal{O}_i(\mathbf{N}) \cup \mathcal{O}_j(\mathbf{M}) \cup \mathcal{O}_u(\mathbf{N} \circ \rho) \cup \mathcal{O}_v(\mathbf{M} \circ \rho), \quad (10)$$

hence, 16 different subsets of operational identities: $\{\mathcal{O}_{ijuv}(\mathcal{B})\}_{ijuv \in \{a,t\}^4}$. Clearly, we have the inclusion relations:

$$\begin{aligned} \mathcal{O}_{aaaa}(\mathcal{B}) &\supseteq \mathcal{O}_{aaat}(\mathcal{B}), \mathcal{O}_{aata}(\mathcal{B}) \supseteq \mathcal{O}_{aatt}(\mathcal{B}) \\ &\supseteq \mathcal{O}_{attt}(\mathcal{B}), \mathcal{O}_{tatt}(\mathcal{B}) \supseteq \mathcal{O}_{tttt}(\mathcal{B}), \end{aligned} \quad (11)$$

which will be useful later. The full set of operational identities, $\mathcal{O}_{aaaa}(\mathcal{B})$, was studied in Ref. [35]. In this Letter, we focus on the four cases of $\mathcal{O}_{aatt}(\mathcal{B})$, $\mathcal{O}_{attt}(\mathcal{B})$, $\mathcal{O}_{tatt}(\mathcal{B})$ and $\mathcal{O}_{tttt}(\mathcal{B})$, as they relate respectively to the separable-entangled, unsteerable-steerable (in the $A \rightarrow B$ and the $B \rightarrow A$ directions) and local-nonlocal boundary among bipartite states. Other subsets are also of interest: $\mathcal{O}_{aaat}(\mathcal{B})$, for instance, characterizes those bipartite states that can prepare ensembles of nonclassical states [38] and has been implicitly studied in [32].

Definition 1. Consider an $(\mathbf{N}, \mathbf{M}, \rho)$ Bell scenario \mathcal{B} and a subset of operational identities $\mathcal{O}(\mathcal{B})$. The operational statistics $p(ab|xy)$ achieved in this scenario are said to be *NCOM-realizable relative to $\mathcal{O}(\mathcal{B})$* if they can be realized by a diagram-preserving (and hence local) model, as in Eq. (3), while respecting the implications of noncontextuality for the operational identities in $\mathcal{O}(\mathcal{B})$, that is, while respecting the subset of ontological identities in Eqs. (5) and (9) that are picked out by $\mathcal{O}(\mathcal{B})$.

In Ref. [35], the notion of classical explainability of the operational statistics of an experiment—in other words, the notion of NCOM-realizability of these statistics—was leveraged to define a notion of classicality for an *individual process* within an experiment. In the case of a bipartite state, it is defined to be classical if and only if the operational statistics generated from the state and all possible local measurements are classically explainable.

More formally, let ρ denote the bipartite state in question. We denote the *full* set of possible quantum measurements on A and the full set on B by \mathbf{N}^{full} and \mathbf{M}^{full} respectively. The resulting Bell scenario, denoted $\mathcal{B}^{\text{full}} = (\mathbf{N}^{\text{full}}, \mathbf{M}^{\text{full}}, \rho)$, is termed a *measurement-full quantum Bell scenario*. The proposal of Ref. [35], then, can be stated as follows:

Definition 2. Consider the measurement-full Bell scenario $\mathcal{B}^{\text{full}} = (\mathbf{N}^{\text{full}}, \mathbf{M}^{\text{full}}, \rho)$. The bipartite state ρ is said to be *classical* if the operational statistics arising in this scenario are NCOM-realizable relative to $\mathcal{O}_{aaaa}(\mathcal{B}^{\text{full}})$, that is, if the operational statistics lie in \mathcal{NC} .

Now, in the Bell scenario $\mathcal{B}^{\text{full}}$, we can leverage the notion of NCOM-realizability relative to different *subsets* of the full set $\mathcal{O}(\mathcal{B}^{\text{full}}) \subseteq \mathcal{O}_{\text{aaaa}}(\mathcal{B}^{\text{full}})$ to define necessary (but in general not sufficient) conditions for the classicality of an bipartite state within that experiment.

Definition 3. Consider a measurement-full Bell scenario $\mathcal{B}^{\text{full}} = (\mathbf{N}^{\text{full}}, \mathbf{M}^{\text{full}}, \rho)$ and a subset of operational identities $\mathcal{O}(\mathcal{B}^{\text{full}})$. The bipartite state ρ is said to be *classical relative to $\mathcal{O}(\mathcal{B}^{\text{full}})$* if the operational statistics arising in this scenario are NCOM-realizable relative to $\mathcal{O}(\mathcal{B}^{\text{full}})$.

It was shown in [35] that the set of bipartite states that are classical (in the sense of Definition 2) is a strict subset of the separable states. Here, we demonstrate that, within the set of bipartite states, the boundary that is induced by the notion of classicality *relative to various choices of subsets of the full set of operational identities* provides a novel and unified operational definition of the separable-entangled boundary, the steerable-unsteerable boundary, and the local-nonlocal boundary.

Theorem 1. Let $\mathcal{B}^{\text{full}} = (\mathbf{N}^{\text{full}}, \mathbf{M}^{\text{full}}, \rho)$ denote a measurement-full Bell scenario. For the bipartite state ρ , there is an equivalence between the two properties in each of the following pairs:

- (1) classicality relative to $\mathcal{O}_{\text{aatt}}(\mathcal{B}^{\text{full}})$ and separability,
- (2) classicality relative to $\mathcal{O}_{\text{attt}}(\mathcal{B}^{\text{full}})$ and $B \rightarrow A$ unsteerability,
- (3) classicality relative to $\mathcal{O}_{\text{tatt}}(\mathcal{B}^{\text{full}})$ and $A \rightarrow B$ unsteerability,
- (4) classicality relative to $\mathcal{O}_{\text{tttt}}(\mathcal{B}^{\text{full}})$ and locality.

We leave the proof of this theorem to Appendix A. The last case follows directly from the fact that if none of the nontrivial operational identities are leveraged, then the only constraint on the correlations is that of Eq. (3), which is simply LHV-realizability [3].

It is worth noting that in a related work [32], the prepare-measure scenario that arises from steered states in a bipartite Bell scenario is considered. This work demonstrates that in such a scenario, a certain witness of NCOM-nonrealizability in the measurement-full Bell scenario is necessary but not sufficient for witnessing entanglement. The key difference between this and the theorem above lies in the choice of operational identities considered. To be more specific, Ref. [32] effectively considers NCOM-realizability relative to $\mathcal{O}_{\text{aaat}}$, whereas case (1) in Theorem 1 in our work focuses on NCOM-realizability relative to $\mathcal{O}_{\text{aatt}}$. By considering the consequence of noncontextuality for fewer operational identities, our theorem above exactly singles out the separable-entangled divide among bipartite states. By considering more operational identities, the constraints from noncontextuality studied in Ref. [32] are more stringent, and so single out a different divide, between a strict *subset* of the separable states and the complement of this set. This subset of bipartite states can be understood as those that

are not capable of steering to a nonclassical set of unipartite states on B , for the notion of nonclassicality defined in [35, 38]. More formally, we have:

Proposition 1. [32, 38] Let $\mathcal{B}^{\text{full}} = (\mathbf{N}^{\text{full}}, \mathbf{M}^{\text{full}}, \rho)$ denote a measurement-full Bell scenario. For the bipartite state ρ , there is an equivalence between the two properties in each of the following pairs:

- (5) classicality relative to $\mathcal{O}_{\text{aaat}}(\mathcal{B}^{\text{full}})$ and the impossibility of steering to a nonclassical set of states on B ,
- (6) classicality relative to $\mathcal{O}_{\text{aata}}(\mathcal{B}^{\text{full}})$ and the impossibility of steering to a nonclassical set of states on A .

The proof of theorem 1 above proceeds in the same way as the proof of theorem 1 in Ref. [32]. For completeness, we review this proof in Appendix A using our notation.

Whether classicality relative to $\mathcal{O}_{\text{aaat}}(\mathcal{B}^{\text{full}}) \cup \mathcal{O}_{\text{aata}}(\mathcal{B}^{\text{full}})$ is equivalent to classicality relative to $\mathcal{O}_{\text{aaaa}}(\mathcal{B}^{\text{full}})$ (which defines the classical-nonclassical boundary studied in Ref. [35]) is not yet known. This open question was first posed explicitly below Theorem 4 in Ref. [35].

C. Inequalities for Noncontextual Ontological Models in a Bell scenario

Experimentally, one cannot implement *all* local measurements that are deemed possible in quantum theory, and so the local sets of measurements \mathbf{N} and \mathbf{M} in an experimental Bell scenario are necessarily distinct from \mathbf{N}^{full} and \mathbf{M}^{full} . In this section, we consider some particular choices of \mathbf{N} and \mathbf{M} and what these allow in terms of witnessing nonclassicality relative to a set of operational identities.

Consider a Bell scenario with outcomes $a, b \in \{0, \dots, o-1\}$ and settings $x \in \{0, \dots, \Delta_{\mathbf{N}}-1\}$ and $y \in \{0, \dots, \Delta_{\mathbf{M}}-1\}$. The correlations $\{p(ab|xy)\}_{abxy}$ can be viewed as points in the probability space $\mathbf{p} \in \mathbb{R}^{o^2 \Delta_{\mathbf{N}} \Delta_{\mathbf{M}}}$. Bell scenarios are typically analyzed relative to the notion of a local hidden variable (LHV) model [3]. The convex set of all LHV-realizable probability distributions $p(ab|xy)$, formalized in Eq. (3), is known as the *local polytope*, denoted \mathcal{L} . Bell inequalities are the facet inequalities of \mathcal{L} . Because LHV-realizability coincides with NCOM-realizability relative to $\mathcal{O}_{\text{tttt}}$ (i.e., both are defined by Eq. (3)), Bell inequalities can also be seen as the weakest set of noncontextuality inequalities in the bipartite Bell scenario. The simplest and most well-known example of Bell inequalities occurs for $\Delta_{\mathbf{N}} = \Delta_{\mathbf{M}} = o = 2$, leading to the Clauser-Horne-Shimony-Holt (CHSH) inequalities [14, 39]. As it turns out, these are the *only* NC inequalities arising in this scenario (see example 1).

In our discussion, we are interested in a set of correlation polytopes that are defined as the set of correlations that are NCOM-realizable relative to various choices of the set of operational identities. We denote the polytope of correlations that are NCOM-realizable relative to the set \mathcal{O}_{ijuv} of operational identities as \mathcal{NC}_{ijuv} . Given the

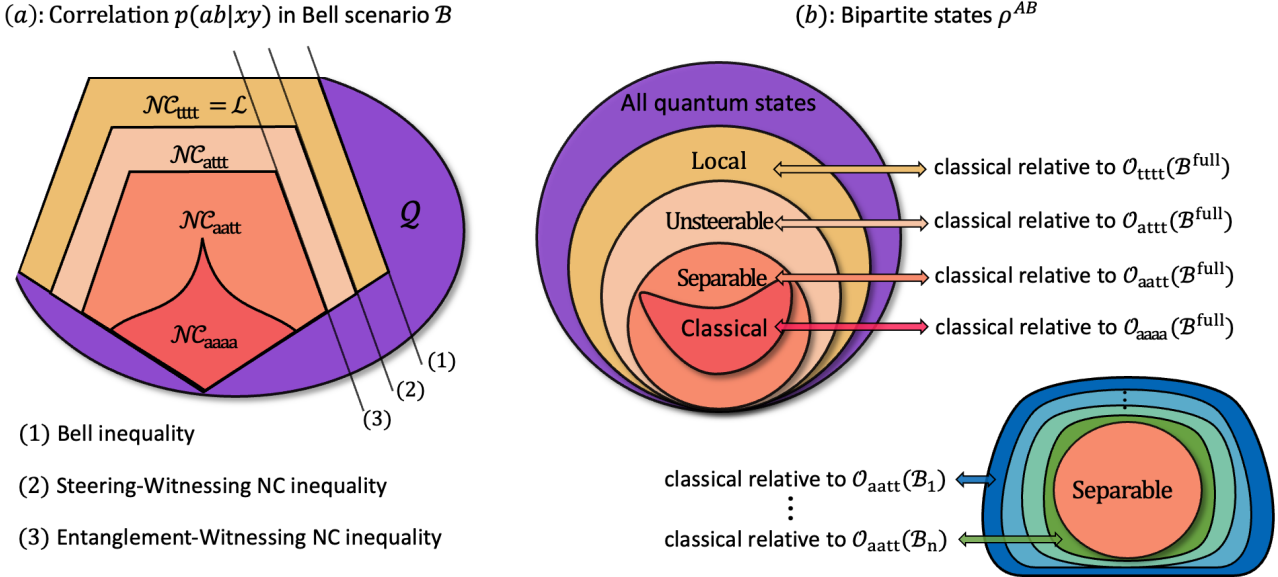


FIG. 2. (a): Given a fixed (N, M, ρ) -Bell scenario \mathcal{B} , we sketch different NCOM-realizable polytopes in the space of operational statistics, where $\mathcal{NC} = \mathcal{NC}_{aaaa} \subseteq \mathcal{NC}_{aatt} \subseteq \mathcal{NC}_{attt} \subseteq \mathcal{NC}_{tttt} = \mathcal{L} \subseteq \mathcal{Q}$. Here, \mathcal{NC}_{aaaa} is defined by considering all operational identities, \mathcal{NC}_{aatt} is defined by considering only nontrivial operational identities on Alice's and on Bob's measurements, \mathcal{NC}_{attt} is defined by not taking into account any nontrivial operational identities, and \mathcal{Q} is the standard set of quantum correlations in a Bell scenario. (b): a bipartite state being classical, separable, unsteerable or local, is equivalent to it being classical relative to $\mathcal{O}_{aaaa}(\mathcal{B}^{\text{full}})$, $\mathcal{O}_{aatt}(\mathcal{B}^{\text{full}})$, $\mathcal{O}_{attt}(\mathcal{B}^{\text{full}})$ or $\mathcal{O}_{tttt}(\mathcal{B}^{\text{full}})$ respectively. (We note that the set of nonclassical separable states is measure zero [35], which is not captured by the Venn diagram.) Insert: Using a sequence of Bell scenarios $\{\mathcal{B}_i = (N_i, M_i, \rho)\}_i$ that limit to the measurement-full Bell scenario with $N_1 \subset \dots \subset N_n \subset \dots \subset N^{\text{full}}$ and $M_1 \subset \dots \subset M_n \subset \dots \subset M^{\text{full}}$, the set of states that are classical relative to $\mathcal{O}_{aatt}(\mathcal{B}_i)$ limits to the set of separable states.

subset inclusion relations of Eq. (11), we have that, for any Bell scenario,

$$\mathcal{NC} = \mathcal{NC}_{aaaa} \subseteq \mathcal{NC}_{aatt} \subseteq \mathcal{NC}_{attt}, \mathcal{NC}_{attt} \subseteq \mathcal{NC}_{tttt} = \mathcal{L}, \quad (12)$$

as depicted schematically in Fig 3 (a). It should be noted that, apart from \mathcal{NC} , each of these sets of correlations is convex, as they are each defined by linear constraints (in the form of Eq. 4) on a convex set \mathcal{L} .

In the following, we focus on the polytope \mathcal{NC}_{aatt} in the context of some particular examples. The numerical procedures underpinning this analysis, namely facet enumeration and polytope membership linear programming, are detailed in Appendix B.

Recall that the local polytope \mathcal{L} depends only on the number of measurements in the sets N and M , denoted Δ_N and Δ_M respectively, and the number of distinct outcomes for each, denoted o . By contrast, the polytope of correlations that are NCOM-realizable relative to the set of operational identities \mathcal{O} depends also on \mathcal{O} . It is convenient to represent \mathcal{O} by its intrinsic geometry, as a shape, the extremal points of which satisfy the linear constraints defined by \mathcal{O} (see Appendix B for full details)

For example, consider the simplest Bell scenario with $\Delta_N = \Delta_M = o = 2$. For any pair of binary-outcome measurements, $M = \{\{M_{a|x}\}_a\}_x$, the full set of opera-

tional identities satisfied by this set of effects is the singleton set consisting of the trivial identity: $M_{0|0} + M_{1|0} = M_{0|1} + M_{1|1}$. The intrinsic geometry of this set of effects is that of a square, since the vertices of the square, denoted $\{\vec{t}_{a,x}\}_{a,x}$, satisfy exactly one linear constraint: $\vec{t}_{0|0} + \vec{t}_{1|0} = \vec{t}_{0|1} + \vec{t}_{1|1}$.

In the following, when we seek to specify the sets of operational identities that hold for Alice's and Bob's local measurements, we do so by specifying the shapes whose internal geometries are defined by the corresponding linear constraints. Denoting this pair of shapes by P and Q respectively, we refer to the corresponding Bell scenario as a (P, Q) Bell scenario.

Example 1. For a (square, square) Bell scenario, which we denote by \mathcal{B}_{ss} , we have $\mathcal{O}_{aatt}(\mathcal{B}_{ss}) = \mathcal{O}_{attt}(\mathcal{B}_{ss}) = \mathcal{O}_{tttt}(\mathcal{B}_{ss})$. It follows that we have a collapse of the hierarchy of correlations in Eq. (12), that is, $\mathcal{NC}_{aatt} = \mathcal{NC}_{attt} = \mathcal{NC}_{tttt}$. Thus, the set of NC inequalities defined by \mathcal{NC}_{aatt} in this scenario is equivalent to the set of CHSH inequalities.

Consequently, to obtain nontrivial NC inequalities that offer new avenues for entanglement certification (i.e., beyond the avenues already offered by Bell tests), it is necessary to consider a Bell scenario with more structure in the local intrinsic geometries of the measurements, and

to show that the inclusions in the hierarchy of Eq. (12) can be made strict.

Our remaining examples take the shapes describing the intrinsic geometries of N and M to be geometric duals of one another. This strategy is motivated by the fact that measurements with specific geometric duality relations achieve the maximal quantum violation of the CHSH inequalities, and the fact that such duality is conjectured to also be optimal for quantum violations of noncontextuality inequalities in prepare-measure scenarios [38]. In particular, we will use certain pairs of regular polyhedra because they potentially allow for a more noise-robust entanglement certification protocol [40] and because their symmetric structures simplify the analysis. The resulting NC inequalities outperform all previously known Bell- and steering-based tests for certifying entanglement in 2-qubit noisy isotropic states, that is, the 1-parameter family of states of the form

$$\rho_{\text{Iso}}^p = p|\Phi^+\rangle\langle\Phi^+| + (1-p)\frac{1}{4}, \quad (13)$$

where $|\Phi^+\rangle = (|00\rangle + |11\rangle)/\sqrt{2}$ is a maximally entangled state shared between Alice and Bob.

Example 2. For an (octahedron, cube) Bell scenario, which is depicted in Fig. 5(a) and which we denote by \mathcal{B}_{oc} , we have $\mathcal{O}_{\text{aatt}}(\mathcal{B}_{\text{oc}}) = \mathcal{O}_{\text{attt}}(\mathcal{B}_{\text{oc}}) \subset \mathcal{O}_{\text{tatt}}(\mathcal{B}_{\text{oc}}) = \mathcal{O}_{\text{tttt}}(\mathcal{B}_{\text{oc}})$. (The equalities are due to the fact that the octahedron, like the square, describes only trivial operational identities, while the strict inclusion is due to the fact that the cube includes some nontrivial operational identities.)

It follows that the inclusion relations in the hierarchy of correlations described in Eq. (12) become: $\mathcal{NC}_{\text{aatt}} = \mathcal{NC}_{\text{attt}} \subset \mathcal{NC}_{\text{tatt}} = \mathcal{NC}_{\text{tttt}}$.

The full characterization of the polytope $\mathcal{NC}_{\text{aatt}}$ is discussed in the Appendix B. It is found to have 336 nontrivial facet inequalities that follow from the principle of noncontextuality, which can be classified into three distinct classes (excluding the trivial nonnegativity constraint), where the elements within each class form an orbit under permutations of the outcome and setting variables. See Table II.

TABLE II. Facet-defining inequalities for the polytope $\mathcal{NC}_{\text{aatt}}$

Inequality	Orbit size
$p(01 22) + p(10 03) - p(11 00) + p(11 21) \geq 0$	144
$p(01 22) + p(10 03) - p(11 00) + p(11 20) \geq 0$	144
$p(01 22) + p(10 03) - p(11 00) + p(11 10)$	48
$-p(11 12) - p(11 20) + p(11 21) + p(11 22) \geq 0$	

In particular, the third class of inequalities can be used to certify entangled two-qubit isotropic states for $p > \frac{1}{\sqrt{3}} \simeq 0.577$, thereby outperforming all certification methods for such states that rely on Bell inequalities based on projective measurements, which only certify entanglement for $p > 1/K_G(3) \in (0.6875, 0.6961)$ [41],

where $K_G(3)$ is the Grothendieck's constant [42]. As a special instance of a Bell inequality, the CHSH inequality derived in Example 1 can only be used to certify entangled two-qubit isotropic states only $p > 1/\sqrt{2} \simeq 0.717$.

However, the range of p that are witnessable via example 2 does *not* exceed the range that are witnessable in principle by steering inequalities, namely, $p \geq 1/2$ [43, 44].

Consequently, to obtain nontrivial NC inequalities that offer avenues for entanglement certification beyond those offered by steering inequalities, it is necessary to consider a Bell scenario with even more structure in the local intrinsic geometries of the measurements. The next example does so.

Example 3. For an (icosahedron,dodecahedron) Bell scenario, which is depicted in Fig. 5(b) and denoted by \mathcal{B}_{id} , we have $\mathcal{O}_{\text{aatt}}(\mathcal{B}_{\text{id}}) \subset \mathcal{O}_{\text{attt}}(\mathcal{B}_{\text{id}})$, $\mathcal{O}_{\text{tatt}}(\mathcal{B}_{\text{id}}) \subset \mathcal{O}_{\text{tttt}}(\mathcal{B}_{\text{id}})$. It follows that the inclusion relations in the hierarchy of correlations described in Eq. (12) become: $\mathcal{NC}_{\text{aatt}} \subset \mathcal{NC}_{\text{attt}}, \mathcal{NC}_{\text{tatt}} \subset \mathcal{NC}_{\text{tttt}}$.

Importantly, there exists the following facet-defining inequality of the polytope $\mathcal{NC}_{\text{aatt}}$:

$$\begin{aligned} \mathcal{I} = & p(00|00) + p(00|01) - (\phi + 1)p(00|02) + \frac{1}{\phi}p(00|03) \\ & + \frac{1}{\phi}p(00|10) + \frac{1}{\phi}p(00|11) - 2p(00|12) + p(00|13) \\ & - p(00|20) - \frac{1}{\phi}p(00|21) + (\phi + 1)p(00|22) - p(00|23) \\ & - \frac{1}{\phi^2}p(10|11) + \frac{1}{\phi}p(10|12) \geq 0, \end{aligned} \quad (14)$$

where $\phi = \frac{\sqrt{5}+1}{2}$. This inequality can be violated by qubit isotropic states for any $p > \sqrt{\frac{1+\phi^2}{3\phi^4}} \approx 0.4195$, and consequently outperforms all entanglement certification methods that rely on steering inequalities.

In principle, by employing pairs of dual polyhedra (P, Q) that successively better approximate the full Bloch sphere, one can push the certification threshold all the way to the separable-entangled boundary as one expects from condition (1) of Theorem 1. For example, using the geodesic and Goldberg polyhedra, with 92 and 180 vertices respectively, we numerically find that entanglement in the noisy 2-qubit isotropic state, ρ_{Iso}^p , can be certified down to $p \gtrsim 0.343$.

In practice, however, experimental complexity limits the number of measurement effects that can be realized, resulting in a trade-off between the tightness of the inequality and the experimental overhead. Therefore, in the following, we focus on the implementation of Example 3, which already outperforms all Bell and steering inequalities in certifying entanglement.

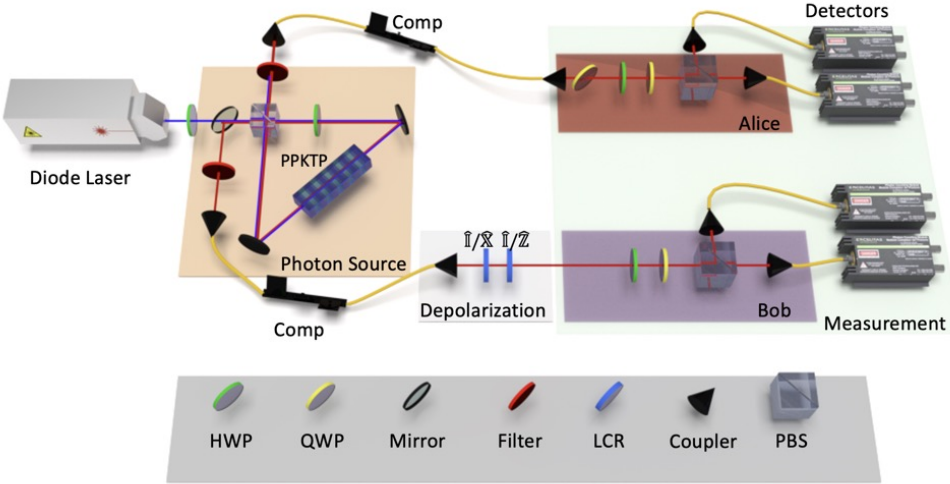


FIG. 3. Schematic of the experiment. Polarization-entangled photon pairs are generated via parametric down-conversion in a Sagnac interferometer [45]. Polarization controllers (Comp) compensate polarization rotations in the single-mode fibres. A pair of computer-controlled liquid crystal phase retarders (LCR) aim to implement arbitrary strength depolarizing channels on one of the photons. Each photon is then directed to separate polarization analyzers—Alice and Bob—where polarization measurements are performed using half-wave plates (HWPs) and quarter-wave plates (QWPs). Coincidence counts are recorded. PPKTP: periodically-poled potassium titanyl phosphate; PBS: polarizing beamsplitter; $\hat{1}$, \hat{X} , \hat{Z} : Pauli gates.

D. Dealing with inexact operational identities

Our approach to entanglement certification assumed that specific operational identities hold among the measurements. Every experimental implementation of a measurement procedure, however, is subject to systematic inaccuracies and statistical noise, such that the operational identities that hold among the realized effects will never exactly match those that hold among the effects that are being targeted. We contend with this problem by generalizing the method of *secondary procedures* from Ref. [46]. We detail this approach and its underlying assumptions in Appendix C 1, and sketch only the main idea here.

If the measurements we are targeting are $\{N_{a|x}\}_x$ and $\{M_{b|y}\}_y$, then the measurements that are in fact realized in the experiment are denoted $\{N_{a|x}^p\}_x$ and $\{M_{b|y}^p\}_y$ and are termed the *primary* measurement procedures. We define the *secondary* measurement procedures, denoted $\{N_{a|x}^s\}_x$ and $\{M_{b|y}^s\}_y$, as follows: (i) each effect is taken to be an element of the convex hull of the primary effects, i.e., $N_{a|x}^s = \sum_{a',x'} u_{a',x'}^{a,x} N_{a'|x'}^p$ and $M_{b|y}^s = \sum_{b',y'} v_{b',y'}^{b,y} M_{b'|y'}^p$, (ii) they are required to satisfy the set of operational identities that are respected by the targeted measurements, i.e., $\mathcal{O}_{\text{all}}(N)$ and $\mathcal{O}_{\text{all}}(M)$, (iii) they maximize a measure of closeness with the primary measurement procedures, namely, the objective functions $C_N = \frac{1}{o\Delta_N} \sum_{a,x} u_{a,x}^{a,x}$ and $C_M = \frac{1}{o\Delta_M} \sum_{b,y} v_{b,y}^{b,y}$. (o, Δ_N, Δ_M are the number of outcomes and settings)

In the end, the *statistics* defined by the secondary mea-

surements $p^s(ab|xy)$ are given as

$$\begin{aligned} p^s(ab|xy) &= \text{Tr}[N_{a|x}^s \otimes M_{b|y}^s \rho^{AB}] \\ &= \sum_{a',b',x',y'} v_{b',y'}^{b,y} u_{a',x'}^{a,x} p(a'b'|x'y'), \end{aligned} \quad (15)$$

where $p(a'b'|x'y')$ are the statistics obtained from the set of primary measurements, i.e., from regularization of the frequencies obtained from the raw data[28, 46] (see Appendix C 2).

As described in the Appendix C 1, the coefficients $u_{a',x'}^{a,x}$ and $v_{b',y'}^{b,y}$ (and hence also the secondary statistics) can be inferred from the primary statistics without any need to characterize the primary and secondary measurements directly. This is the sense in which we are generalizing the method discussed in Ref. [46].

III. EXPERIMENTAL RESULTS

Our experiment tests the NC inequality of Eq. (14) for various choices of the value of the parameter p in the 1-parameter family of 2-qubit states. It uses the photonic setup depicted in Fig. 3. As discussed in depth in the Appendix D, we generate polarization-entangled photons via type-II spontaneous parametric down-conversion in a Sagnac interferometer. These photons are subsequently directed through a controlled depolarization channel by probabilistic mixtures of four Bell states as outlined in the Appendix D 1. The strength of the depolarization transforms the bipartite state into different mixed states

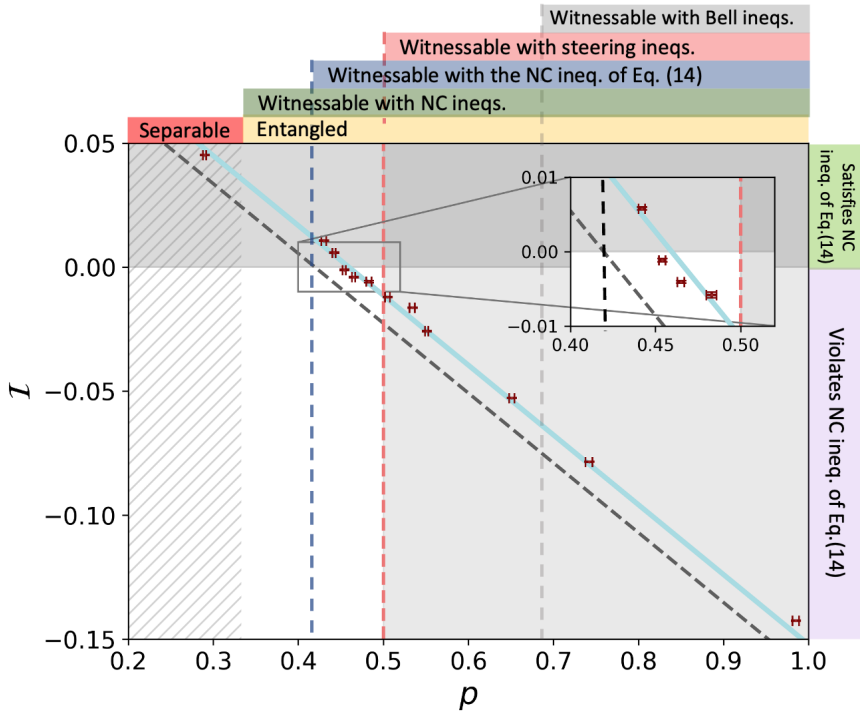


FIG. 4. Experimental violation of the noncontextuality (NC) inequality of Eq. 14, i.e., $\mathcal{I} \geq 0$, as a function of the isotropic-state parameter p . Our experimental data are shown as points with vertical and horizontal error bars, while the ideal case is shown as the diagonal dashed gray line, and the ideal case under 2% white noise in the measurements is shown as a solid blue line. On top of the diagram, we depict the separable-entangled divide, as well as the parameter regimes certifiable by various techniques: general noncontextuality inequalities, the specific noncontextuality inequality used in this work, and steering inequalities. The region in white contains states that simultaneously i) are entangled, ii) are not certifiable by steering (or Bell) inequalities, and iii) are certifiable by noncontextuality inequalities. Three of our experimental data points lie in this white region, demonstrating the advantage of our approach over these prior approaches. Error bars for both \mathcal{I} and p are obtained from 100 trials of Monte Carlo simulation and are depicted. (See Table IV for detailed data.)

closely approximating (with greater than 99% state fidelity) 2-qubit isotropic states with different values of the parameter p (see Eq. (13)) that are separable, entangled, steerable, or nonlocal [6, 8, 43, 44].

In the experiment, we prepared 12 different quantum states ρ_{exp} , each with a measured fidelity to the nearest isotropic state ρ_{iso}^p exceeding 99% (see table IV in Appendix D), where the parameter p will be used to represent the state we prepared. The NC inequality of Eq. (14) requires Alice's and Bob's measurements to have the intrinsic geometry of an icosahedron and dodecahedron respectively. We target a regular icosahedron and a regular dodecahedron inscribed in the Bloch sphere for Alice and Bob's measurements respectively, as depicted in Fig. 5 (see Eq. B5 in the Appendix B for a precise definition). This corresponds to implementing 6 projective binary-outcome measurements on Alice's photon and 10 on Bob's. These measurements clearly satisfy the relevant operational identities, and are predicted to violate the NC inequality of Eq. (14). They are implemented using a combination of half-wave plates (HWP), quarter-wave plates (QWP), and polarization beam splitters (PBS).

For each of the 12 states, we implemented 60 distinct pairs of measurement settings (6 on Alice and 10 on Bob). In 2 hours, each pair of settings accumulated on the order of 2×10^6 twofold coincidence counts (consisting of four coincidence pairs), which are denoted as the raw count statistics $N(ab|xy)$.

Imperfections in experimental implementation, such as polarization optics quality, fiber drift, and laser power drift are unavoidable. Additionally, the raw count statistics $N(ab|xy)$ represent finite samples from the true probability distribution, and directly normalizing them may yield a distribution that is not physically realizable, even within a generalized probabilistic theory (GPT) [47, 48]. For example, statistical fluctuations can result in violations of no-signaling conditions. To address this, the raw counts are fitted to a probability distribution $p(ab|xy)$ that is reproducible either by quantum theory or, more generally, by a GPT of dimension 4×4 , using a total weighted least squares method [49].

From the resulting primary statistics $p(ab|xy)$, we construct secondary statistics $p^s(ab|xy)$ via the technique discussed in the previous section. For the quantities $C_N = \frac{1}{\sigma \Delta_N} \sum_{a,x} u_{a,x}^{a,x}$ and $C_M = \frac{1}{\sigma \Delta_M} \sum_{b,y} v_{b,y}^{b,y}$, we

achieve an average of 0.98 and 0.96 (see Table VI), which confirms that the secondary statistics remain very close to the primary statistics (effectively introducing $\sim 2\%$ white noise to the measurements.)

Experimental values of the quantity \mathcal{I} are presented in Fig. 4, where error bars are obtained via Monte Carlo simulations assuming Poisson count statistics. Violations of the inequality in Eq. (14) are observed for all set-ups that correspond to isotropic states with estimated $p > 0.43$, including those with $p < 0.5$, for which it is known that their entanglement cannot be certified by steering inequalities [35].

Although our experimentally prepared states achieve fidelities above 99% with the nearest isotropic state, this only guarantees that they are *close to* unsteerable states but does not guarantee that they are in fact unsteerable (because it remains an open question whether proximity to an unsteerable isotropic state implies unsteerability). To address this, we directly assess whether each of the bipartite states prepared in our experiment admit a local-hidden-state (LHS) model by solving a semidefinite program (SDP) (see Appendix E). This analysis showed that the state associated to parameter value $p = 0.483$ cannot be certified as unsteerable, but that the states associated to parameter values $p = 0.454$ and $p = 0.465$ are certified as unsteerable (see table IV and discussion in Appendix E).

IV. COMPARISON WITH ALTERNATIVE ENTANGLEMENT CERTIFICATION APPROACHES

The entanglement certification method presented above can be systematically extended to all entangled states by constructing appropriate noncontextuality inequalities in Bell scenarios with larger numbers of local measurements, as guaranteed by Theorem 1. We now discuss the features of our entanglement certification technique relative to pre-existing techniques, a summary of which can be found in Table I.

Witnessing entanglement by implementing a separability test on a state obtained from quantum state tomography requires a prior characterization of one's measurements. Such a prior characterization is also required for estimating entanglement witnesses. By contrast, our approach resembles that of GPT tomography [26, 50] and gate-set tomography [27, 33], which do not require a prior characterization of any subset of the procedures in the experiment, but rather infer characterizations of all the procedures from how they interact, i.e., in a bootstrap fashion.

For the Bell scenario, both GPT tomography and gate-set tomography would not return a unique output for the bipartite state and for the local effects, but rather a set of possible triples of theses, related by an invertible linear transformation. Following Ref. [27], we refer to this as a tomographic *gauge freedom*. The most obvious way to

certify entanglement of the bipartite state in this case is to implement a separability test for all possible choices of gauge.

Our approach also begins, as in bootstrap tomography, by regularizing the raw frequencies into a valid probability distribution, and then estimating the state and local effects in a particular gauge. However, it differs in how we use this output to certify entanglement. Rather than doing a separability test after an optimization over gauge, we use the gauge-dependent state and local effects to compute the probability distribution that these predict under the Born rule, which is a gauge-independent quantity. Finally, we test our NC inequality on this probability distribution. Our technique consequently provides the possibility of certifying entanglement without requiring any optimization over gauge and indeed without even requiring a description of the full gauge freedom of the state and local effects.³

Another technique for certifying entanglement that is gauge-independent and requires no prior characterization of the measurements is to use violations of Bell inequalities (e.g., in the device-independent paradigm [3]). As argued in Ref. [28], the rigorous implementation of this approach requires regularizing one's raw data from a Bell test to the nearest nonsignaling probability distribution, and then testing the fit data using some Bell inequality. These device-independent tests have an advantage over the technique described here: they do not require the sets of local effects to be tomographically complete, while our technique does. However, the price Bell tests pay for this advantage is that they can only certify entanglement in a strict subset of all entangled states [6].

A final approach to verifying entanglement is to incorporate causal compatibility constraints within more elaborate causal networks. As shown in Ref. [29], such methods can in principle certify entanglement in *any* entangled state, while retaining the advantages of being a gauge-independent technique requiring no prior characterization of the measurements. However, these approaches require network structures that are more experimentally complex than that of the Bell scenario; in particular, they require additional entangled sources beyond the one being characterized.

Before concluding, we remark that our approach can be straightforwardly extended to the multipartite scenario. For example, the certification of all multipartite entangled states can be achieved by considering NCOM-realizability where the set of operational identities that is used includes all identities on each set of local measurements.

³ It should be noted that fixing a tomographic gauge (rather than optimizing over it) can lead to estimates of quantities of interest that may be off by orders of magnitude from the true value [33].

V. DISCUSSION

On the foundational side, we showed that the inequalities witnessing entanglement, steerability, and nonlocality are obtained from NC inequalities when the principle of noncontextuality is applied to a hierarchy of subsets of the full set of operational identities. This hierarchy also offers an alternative *definition* of entanglement, steering, and nonlocality in terms of NCOM-nonrealizability for the measurement-full Bell scenario. It can furthermore be adapted to obtain necessary conditions for nonclassicality in types of processes beyond bipartite states, including channels, instruments, and multipartite states, as initially outlined in Ref. [35].

On the technical side, our noncontextuality inequalities can be directly translated into an experimentally implementable entanglement certification protocol. Uniquely among techniques for doing so, ours offers the possibility of realizing all of the following features at once: requiring no prior characterization of the measurement devices, delivering a verdict based on quantities that are gauge-independent, being implementable using only the causal structure of a standard bipartite Bell scenario, and being able in principle to witness the entanglement of any entangled state.

One clear avenue for future work is to use our methods to identify simple and tractable noncontextuality inequalities that correspond to necessary conditions for nonclassicality (such as witnessing entanglement) in other families of states (beyond 2-qubit isotropic states), as well as to do so for more general types of processes such as quantum channels and instruments. Another frontier is to reexamine the assumptions concerning tomographic completeness that are required for experimental tests of NC inequalities [51, 52]. Finally, our novel approach to obtaining necessary conditions for nonclassicality might also lead to novel ways of *quantifying* nonclassicality.

VI. ACKNOWLEDGEMENTS

We thank Yilè Ying, Emanuele Polino, Elie Wolfe and Yeong-Cherng Liang for useful discussions. The research was supported in part by the Natural Sciences and Engineering Research Council of Canada (NSERC), the NSERC-Alliance Hyperspace project, Industry Canada, the Canada Foundation for Innovation (CFI), Canada Excellence Research Chair (CERC) program and the Canada First Research Excellence Fund (CFREF). D.S. and R.W.S. were supported by Perimeter Institute for Theoretical Physics. Research at Perimeter Institute is supported in part by the Government of Canada through the Department of Innovation, Science and Economic Development and by the Province of Ontario through the Ministry of Colleges and Universities.

VII. CODE AVAILABILITY

The code needed to reproduce the main results is available on GitHub [53].

VIII. AUTHOR CONTRIBUTIONS

Y.Z., D.S., and R.W.S. conceived the theory. Y.Z. developed the theory. Y.Z., J.S., and K.J.R. developed the experiment. J.S., C.R., and L.J.M. built the experiment and collected the data. Y.Z. and J.S. analyzed the data. Y.Z., D.S., J.S., T.J., K.J.R. and R.W.S. composed the manuscript.

Appendix A: Proof of Theorem 1 and Proposition 1

Below we provide a detailed proof of Theorem 1 and Proposition 1 from the main text. We begin by recalling the notion of a classical preparation (or classical set of states) introduced in [35].

Definition 4. [35] In measurement-full prepare-and-measure scenario $\mathcal{P}^{\text{full}} = (\mathcal{M}^{\text{full}}, \mathcal{P})$. The multi-preparation $\mathcal{P} = \{\{\tilde{\rho}_{a|x}^B\}_a\}_x$ (a set of unnormalized state) is said to be *classical* if the operational statistics arising in this scenario are NCOM-realizable relative to $\mathcal{O}_{\text{all}}(\mathcal{M}^{\text{full}}) \cup \mathcal{O}_{\text{all}}(\mathcal{P})$.

Theorem 1 and Proposition 1. Let $\mathcal{B}^{\text{full}} = (\mathcal{N}^{\text{full}}, \mathcal{M}^{\text{full}}, \rho)$ denote a measurement-full Bell scenario. For the bipartite state ρ , there is an equivalence between the two properties in each of the following pairs:

- (1) classicality relative to $\mathcal{O}_{\text{aatt}}(\mathcal{B}^{\text{full}})$ and separability,
- (2) classicality relative to $\mathcal{O}_{\text{attt}}(\mathcal{B}^{\text{full}})$ and $B \rightarrow A$ unsteerability,
- (3) classicality relative to $\mathcal{O}_{\text{tatt}}(\mathcal{B}^{\text{full}})$ and $A \rightarrow B$ unsteerability,
- (4) classicality relative to $\mathcal{O}_{\text{tttt}}(\mathcal{B}^{\text{full}})$ and locality,
- (5) classicality relative to $\mathcal{O}_{\text{aaat}}(\mathcal{B}^{\text{full}})$ and the impossibility of steering nonclassical set of states on B ,
- (6) classicality relative to $\mathcal{O}_{\text{aata}}(\mathcal{B}^{\text{full}})$ and the impossibility of steering nonclassical set of states on A .

Proof. The core of the proof is to apply the generalized Gleason theorem [54] iteratively to the different components of the ontological model. We start with Case (2) of Theorem 1, then treat Case (1). Cases (3) and (4) follow directly from these arguments, and Cases (5) and (6) will be proved at the end.

Case (2): If a bipartite state ρ^{AB} is classical relative to $\mathcal{O}_{\text{attt}}(\mathcal{B}^{\text{full}})$, by definition 3, the operational statistics $p(ab|xy)$ it generates with all local POVMs $\{N_{a|x}\}_a \in \mathcal{N}^{\text{full}}$ and $\{M_{b|y}\}_b \in \mathcal{M}^{\text{full}}$ should be NCOM-realizable relative to $\mathcal{O}_{\text{attt}}(\mathcal{B}^{\text{full}})$ per definition 1. More specifically,

one can write

$$p(ab|xy) = \text{Tr}[(N_{a|x} \otimes M_{b|y})\rho^{AB}] = \sum_{\lambda_A \lambda_B} p(\lambda_A \lambda_B)p(a|x, \lambda_A)p(b|y, \lambda_B) \quad (\text{A1})$$

the assumption of noncontextuality applied to $\mathcal{O}_{\text{all}}(\mathbf{N}^{\text{full}})$ implies that the response function $p(a|x, \lambda)$ is a linear function of $N_{a|x}$. The generalized Gleason's theorem then ensures the existence a unique density operator ρ_{λ_A} such that $p(a|x, \lambda_A) = \text{Tr}[\rho_{\lambda_A} N_{a|x}]$. Defining the steering assemblage $\{\tilde{\rho}_{b|y}^A = \text{Tr}[(\mathbb{1} \otimes M_{b|y})\rho^{AB}]\}_y$, one has

$$\begin{aligned} p(ab|xy) &= \text{Tr}[\tilde{\rho}_{b|y}^A N_{a|x}] \\ &= \sum_{\lambda_A \lambda_B} p(\lambda_A \lambda_B)p(b|y, \lambda_B)\text{Tr}[N_{a|x}\rho_{\lambda_A}] \\ \Rightarrow \tilde{\rho}_{b|y}^A &= \sum_{\lambda_A \lambda_B} p(\lambda_A \lambda_B)p(b|y, \lambda_B)\rho_{\lambda_A}, \end{aligned} \quad (\text{A2})$$

where in the last line, we use the fact that the set of all measurement \mathbf{N}^{full} is tomographically complete. This decomposition is a local hidden state model for the assemblage, so the state ρ^{AB} is unsteerable from B to A .

The reverse direction follows directly, if a bipartite state ρ^{AB} is unsteerable, by definition, the state assemblage $\{\tilde{\rho}_{b|y}^A = \text{Tr}[(\mathbb{1} \otimes M_{b|y})\rho^{AB}]\}_y, \forall \{M_{b|y}\}_y \in \mathbf{M}^{\text{full}}$ should admits a local hidden state model [5]:

$$\tilde{\rho}_{b|y}^A = \sum_{\lambda_A} p(\lambda_A)p(b|y, \lambda_A)\rho_{\lambda_A}, \quad (\text{A3})$$

with $\sum_{\lambda_A} p(\lambda_A) = \sum_b p(b|y, \lambda_A) = 1$, $p(\lambda_A), p(b|y, \lambda_A) \geq 0$ and $\rho_{\lambda_A} \geq \mathbb{0}$. Therefore, the operational statistics $p(ab|xy)$ it generates with all local POVMs $\{N_{a|x}\}_a \in \mathbf{N}^{\text{full}}$ and $\{M_{b|y}\}_y \in \mathbf{M}^{\text{full}}$ must be NCOM-realizable relative to $\mathcal{O}_{\text{aatt}}(\mathcal{B}^{\text{full}})$, since one can define

$$p(ab|xy) := \text{Tr}[\tilde{\rho}_{b|y}^A N_{a|x}] = \sum_{\lambda_A} p(\lambda_A)p(b|y, \lambda_A)\text{Tr}[N_{a|x}\rho_{\lambda_A}]$$

where $\sum_b p(b|y, \lambda_A) = 1$ and satisfies the trivial operational identities $\mathcal{O}_{\text{triv}}(\mathbf{M}^{\text{full}})$, while one can define $p(a|x, \lambda_A) := \text{Tr}[N_{a|x}\rho_{\lambda_A}]$, which is a nonnegative linear function of all $N_{a|x} \in \mathbf{N}^{\text{full}}$ that satisfies $\mathcal{O}_{\text{all}}(\mathbf{N}^{\text{full}})$.

Case (1): If a bipartite state ρ^{AB} is classical relative to $\mathcal{O}_{\text{aatt}}(\mathcal{B}^{\text{full}})$, by definition 3, the operational statistics $p(ab|xy)$ it generates with all local POVMs $\{N_{a|x}\}_a \in \mathbf{N}^{\text{full}}$ and $\{M_{b|y}\}_y \in \mathbf{M}^{\text{full}}$ should be NCOM-realizable relative to $\mathcal{O}_{\text{aatt}}(\mathcal{B}^{\text{full}})$ per definition 1.

Specifically, its operational statistics $p(ab|xy)$ should be realizable by Eq. A1, where the assumption of noncontextuality applied to $\mathcal{O}_{\text{all}}(\mathbf{N}^{\text{full}})$ and $\mathcal{O}_{\text{all}}(\mathbf{M}^{\text{full}})$ implies that the response function $p(a|x, \lambda_A)$ is a linear function of the effect $N_{a|x}$ and that $p(b|y, \lambda_B)$ is a linear function of $M_{b|y}$. The generalized Gleason's theorem then guarantees the existence of unique density operators ρ_{λ_A} and

σ_{λ_B} such that we can write $p(a|x, \lambda_A) = \text{Tr}[\rho_{\lambda_A} N_{a|x}]$ and $p(b|y, \lambda_B) = \text{Tr}[\sigma_{\lambda_B} M_{b|y}]$. Plugging these in to Eq. A1, for every pairs of POVMs $\{N_{a|x}\}_a$ and $\{M_{b|y}\}_b$, we have

$$\begin{aligned} &\text{Tr}[(N_{a|x} \otimes M_{b|y})\rho^{AB}] \\ &= \sum_{\lambda_A \lambda_B} p(\lambda_A \lambda_B)\text{Tr}[N_{a|x}\rho_{\lambda_A}]\text{Tr}[M_{b|y}\sigma_{\lambda_B}] \\ \Rightarrow \rho^{AB} &= \sum_{\lambda_A \lambda_B} p(\lambda_A \lambda_B)\rho_{\lambda_A} \otimes \sigma_{\lambda_B}, \end{aligned} \quad (\text{A4})$$

where in the last line, we used the fact that the set of all product measurements is tomographically complete for the space of quantum states. So the state is separable.

The reverse direction is straightforward, as one only needs to show that the operational statistics arising from a separable state $\rho^{AB} = \sum_{\lambda_A \lambda_B} p(\lambda_A \lambda_B)\rho_{\lambda_A} \otimes \sigma_{\lambda_B}$ along with all POVMs $\{N_{a|x}\}_a \in \mathbf{N}^{\text{all}}$ and $\{M_{b|y}\}_b \in \mathbf{M}^{\text{all}}$ are NCOM-realizable relative to $\mathcal{O}_{\text{aatt}}(\mathcal{B}^{\text{full}})$. This can be met by defining the response functions $p(a|x, \lambda_A) = \text{Tr}[\rho_{\lambda_A} N_{a|x}]$ and $p(b|y, \lambda_B) = \text{Tr}[\sigma_{\lambda_B} M_{b|y}]$, which clearly are linear maps from POVMs to their ontological representations and respect $\mathcal{O}_{\text{all}}(\mathbf{N}^{\text{full}})$ and $\mathcal{O}_{\text{all}}(\mathbf{M}^{\text{full}})$.

Now, we will prove case (5), case (6) follows similarly.

Case (5): If a bipartite state ρ^{AB} is classical relative to $\mathcal{O}_{\text{aatt}}(\mathcal{B}^{\text{full}})$, by definition 3, the operational statistics $p(ab|xy)$ it generates with all local POVMs $\{N_{a|x}\}_a \in \mathbf{N}^{\text{full}}$ and $\{M_{b|y}\}_b \in \mathbf{M}^{\text{full}}$ should be NCOM-realizable relative to $\mathcal{O}_{\text{aatt}}(\mathcal{B}^{\text{full}})$ per definition 1. Specifically, its operational statistics $p(ab|xy)$ should be realizable by Eq. A1 and the assumption of noncontextuality applied to $\mathcal{O}_{\text{all}}(\mathbf{M}^{\text{full}})$ implies the existence of unique density operators σ_{λ_B} such that we can write $p(b|y, \lambda_B) = \text{Tr}[\sigma_{\lambda_B} M_{b|y}]$. Moreover, the assumption of noncontextuality applied to $\mathcal{O}_{\text{all}}(\mathbf{N}^{\text{full}} \circ \rho)$ implies the existence of a Hermitian operator H_{λ_B} such that $\sum_{\lambda_A} p(a|x, \lambda_A)p(\lambda_A \lambda_B) = \text{Tr}[(N_{a|x} \otimes H_{\lambda_B})\rho^{AB}] = \text{Tr}[H_{\lambda_B} \tilde{\rho}_{a|x}^B] \geq 0$, where we definition of $\tilde{\rho}_{a|x}^B$ in Eq. 6a. Combining these facts, we have

$$\begin{aligned} \text{Tr}[\tilde{\rho}_{a|x}^B M_{b|y}] &= \text{Tr}[(N_{a|x} \otimes M_{b|y})\rho^{AB}] \\ &= \sum_{\lambda_A \lambda_B} p(\lambda_A \lambda_B)p(a|x, \lambda_A)p(b|y, \lambda_B) \\ &= \sum_{\lambda_B} \text{Tr}[H_{\lambda_B} \tilde{\rho}_{a|x}^B] \text{Tr}[M_{b|y} \sigma_{\lambda_B}] \\ \Rightarrow \tilde{\rho}_{a|x}^B &= \sum_{\lambda_B} \text{Tr}[H_{\lambda_B} \tilde{\rho}_{a|x}^B] \sigma_{\lambda_B}, \end{aligned} \quad (\text{A5})$$

where in the last line, we used the fact that the set of all measurements is tomographically complete for the space of quantum states. According to Theorem 2 in [35], decomposition in Eq. A5 ensures that the assemblage $\{\tilde{\rho}_{a|x}^B\}_x$ is classical.

For the reverse direction, if the state assemblage $\{\tilde{\rho}_{a|x}^B := \text{Tr}[(N_{a|x} \otimes \mathbb{1})\rho^{AB}]\}_x$ defined for $\forall \{N_{a|x}\}_a \in \mathbf{N}^{\text{full}}$ is classical, according to Theorem 2 in [35], one can

find a frame representation $\tilde{\rho}_{a|x}^B = \sum_{\lambda_B} \text{Tr}[H_{\lambda_B} \tilde{\rho}_{a|x}^B] \sigma_{\lambda_B}$ with $\sigma_{\lambda_B} \geq 0$ and $\text{Tr}[H_{\lambda_B} \tilde{\rho}_{a|x}^B] \geq 0$ for all λ_B .

Therefore, combining with all $\{M_{b|y}\}_b \in \mathcal{M}^{\text{full}}$ one has:

$$\begin{aligned} \text{Tr}[(N_{a|x} \otimes M_{b|y}) \rho^{AB}] &= \text{Tr}[\tilde{\rho}_{a|x}^B M_{b|y}] \\ &= \sum_{\lambda_B} \text{Tr}[H_{\lambda_B} \tilde{\rho}_{a|x}^B] \text{Tr}[M_{b|y} \sigma_{\lambda_B}] \\ &= \sum_{\lambda_B} \text{Tr}[(N_{a|x} \otimes H_{\lambda_B}) \rho^{AB}] \text{Tr}[M_{b|y} \sigma_{\lambda_B}] \\ &:= \sum_{\lambda_B} \text{Tr}[N_{a|x} \tau_{\lambda_B}] \text{Tr}[M_{b|y} \sigma_{\lambda_B}] \end{aligned} \quad (\text{A6})$$

In the last equality, we define $\tau_{\lambda_B} := \text{Tr}_B[(\mathbb{1} \otimes H_{\lambda_B}) \rho^{AB}]$, where $\tau_{\lambda_B} \geq 0$ is ensured because $\text{Tr}[N_{a|x} \tau_{\lambda_B}] = \text{Tr}[H_{\lambda_B} \tilde{\rho}_{a|x}^B] \geq 0$ for all $\{N_{a|x}\}_a \in \mathcal{N}^{\text{full}}$. Hence, one can simply define $p(\lambda_A \lambda_B) = \delta_{\lambda_A \lambda_B}$, $p(b|y, \lambda_B) = \text{Tr}[M_{b|y} \sigma_{\lambda_B}]$ and $p(a|x, \lambda_A) = \text{Tr}[N_{a|x} \tau_{\lambda_A}]$, respectively, as the ontological representation for each process in the ontological model.

Checking that this model satisfies every noncontextuality constraint in $\mathcal{O}_{\text{aatt}}(\mathcal{B}^{\text{full}})$ is then straightforward. The constraints in $\mathcal{O}_{\text{all}}(\mathcal{N}^{\text{full}})$ and $\mathcal{O}_{\text{all}}(\mathcal{M}^{\text{full}})$ hold trivially, since $\tau_{\lambda_A}, \sigma_{\lambda_B} \geq 0$. For $\mathcal{O}_{\text{all}}(\mathcal{N}^{\text{full}} \circ \rho)$, note that $\sum_{\lambda_A} p(\lambda_A \lambda_B) p(a|x, \lambda_A) = \text{Tr}[N_{a|x} \tau_{\lambda_B}] = \text{Tr}[(N_{a|x} \otimes H_{\lambda_B}) \rho^{AB}] = \text{Tr}[\tilde{\rho}_{a|x}^B H_{\lambda_B}] \geq 0$, hence the composition map is linear in the assemblage $\{\{N_{a|x} \circ \rho^{AB} = \tilde{\rho}_{a|x}^B\}_a\}_x$ for all $\{N_{a|x}\}_a \in \mathcal{N}^{\text{full}}$. Therefore, we have a valid ontological model that respects $\mathcal{O}_{\text{aatt}}(\mathcal{B}^{\text{full}})$ \square

Appendix B: Deriving the noncontextuality inequalities from the main text

Consider a Bell scenario $\mathcal{B} = (\mathcal{N}, \mathcal{M}, \rho)$ where Alice and Bob each perform $\Delta_{\mathcal{N}}$ and $\Delta_{\mathcal{M}}$ different o -outcome measurements, respectively. One can visualize the operational statistics $p(ab|xy)$ as a point $\vec{p} := \{p(ab|xy)\}_{a,b,x,y} \in \mathbb{R}^{o^2 \Delta_{\mathcal{N}} \Delta_{\mathcal{M}}}$. The set of all the operational statistics that are NCOM-realizable relative to $\mathcal{O}_{\text{aatt}}(\mathcal{B})$ forms a polytope in this space, which we denote as $\mathcal{NC}_{\text{aatt}}$.

As stated in the main text (and illustrated by Example 1), a set of operational identities $\mathcal{O}_{\text{all}}(\mathcal{N})$ can be represented by a geometric object—specifically, a polytope. Concretely, each operational identity is a set of coefficients $\mathcal{O}_{\text{all}}(\mathcal{N}) = \{\{\alpha_{a,x}\}_{a,x}\}$, so one can associate to it a polytope P whose vertices are indexed by $\{\vec{t}_{a,x}\}$ satisfying all the equalities $\sum_{a,x} \alpha_{a,x} \vec{t}_{a,x} = \vec{0}$ and no other equalities. Conversely, given a polytope P with vertices indexed by $\vec{t}_{a,x}$, one can pick an arbitrary coordinate to represent them and define the set of operational identities via the equalities they satisfy: $\mathcal{O}_{\text{all}}(\mathcal{N}) = \{\{\alpha_{a,x}\} | \sum_{a,x} \alpha_{a,x} \vec{t}_{a,x} = \vec{0}\}$ associated with P . (An explicit method for computing these coefficients

from a given set of vectors is given in Appendix A of Ref. [55].) This duality allows us to visualize operational constraints in purely geometric terms (as we did in the main text).

The extreme points $\vec{v} \in \mathcal{NC}_{\text{aatt}}$ are those that can be obtained from the extreme operational statistics, i.e., those of the form $p(ab|xy) = \sum_{\lambda_A \lambda_B} p(\lambda_A \lambda_B) p(a|x, \lambda_A) p(b|y, \lambda_B)$ when $p(\lambda_A \lambda_B) \in \{0, 1\}$ and when the response functions $\{p(a|x, \lambda_A)\}_{a,x}$ and $\{p(b|y, \lambda_B)\}_{b,y}$ are also extremal within the *noncontextual-measurement-assignment polytope* [38, 56]. The noncontextual-measurement-assignment polytope $\mathbb{P}_{\mathcal{M}}$ is formally defined as a collection of points $\vec{u} := \{p(b|y)\}_{b,y}$ such that

$$(i) \quad p(b|y) \geq 0 \quad \forall b, y \quad (\text{B1a})$$

$$(ii) \quad \sum_b p(b|y) = 1 \quad \forall y \quad (\text{B1b})$$

$$(iii) \quad \sum_{b,y} \beta_{b,y} p(b|y) = 0 \quad \forall \{\beta_{b,y}\} \in \mathcal{O}_{\text{all}}(\mathcal{M}). \quad (\text{B1c})$$

Therefore, all extreme points $\vec{v} \in \mathcal{NC}_{\text{aatt}}$ can be obtained from the extreme points $\vec{u} \in \mathbb{P}_{\mathcal{M}}$ and $\vec{w} \in \mathbb{P}_{\mathcal{N}}$ via $\vec{v} = \vec{u} \otimes \vec{w}$.

For simple cases, one can completely characterize the polytope $\mathcal{NC}_{\text{aatt}}$ by enumerating all the extreme points in $\{\vec{v} = \vec{u} \otimes \vec{w}\}$ with $\vec{u} \in \mathbb{P}_{\mathcal{N}}$ and $\vec{w} \in \mathbb{P}_{\mathcal{M}}$. Taking the (octahedron, cube) Bell scenario of Example 2, for instance: for measurements $\mathcal{N} = \{N_{a|x}\}_a$ and $\mathcal{M} = \{M_{b|y}\}_b$ for $a, b \in [0, 1]$, $x \in [0, 1, 2]$ and $y \in [0, 1, 2, 3]$ having cubic and octahedral symmetry for their effects, we find that the $\mathcal{NC}_{\text{aatt}}$ polytope lives in a 15-dimensional subspace of the full 48-dimensional probability space ($d = o^2 \Delta_{\mathcal{N}} \Delta_{\mathcal{M}} = 48$), where the spanned dimension is reduced by equality constraints coming from normalization, no-signaling, and noncontextuality.

In the 15-dimensional subspace, we find that the facet inequalities coming from noncontextuality number 336 in total, which can be classified into three equivalence classes under permutations of values of inputs and outputs that obey the same cubic and octahedral symmetry. We therefore explicitly list a single representative inequality, as in Table II. Importantly, one can show that, for isotropic state ρ_{Iso}^p with $p > \frac{1}{\sqrt{3}}$, the last inequality can be violated using the following measurements that respect operational identities $\mathcal{O}_{\mathcal{N}}$ and $\mathcal{O}_{\mathcal{M}}$ in the (octahedron, cube) Bell scenario: $M_{a|x} = \frac{1}{2}(\mathbb{1} + (-1)^a \hat{m}_x \cdot \vec{\sigma})$ and $N_{b|y} = \frac{1}{2}(\mathbb{1} + (-1)^b \hat{n}_y \cdot \vec{\sigma})$

$$\begin{aligned} \hat{m}_0 &= [1, 0, 0], \quad \hat{m}_1 = [0, 1, 0], \quad \hat{m}_2 = [0, 0, 1] \\ \hat{n}_0 &= \frac{1}{\sqrt{3}}[1, 1, 1], \quad \hat{n}_1 = \frac{1}{\sqrt{3}}[1, 1, -1], \\ \hat{n}_2 &= \frac{1}{\sqrt{3}}[1, -1, 1], \quad \hat{n}_3 = \frac{1}{\sqrt{3}}[1, -1, -1]. \end{aligned} \quad (\text{B2})$$

Moving to a more complicated scenario, the computational complexity of the facet enumeration problem grows

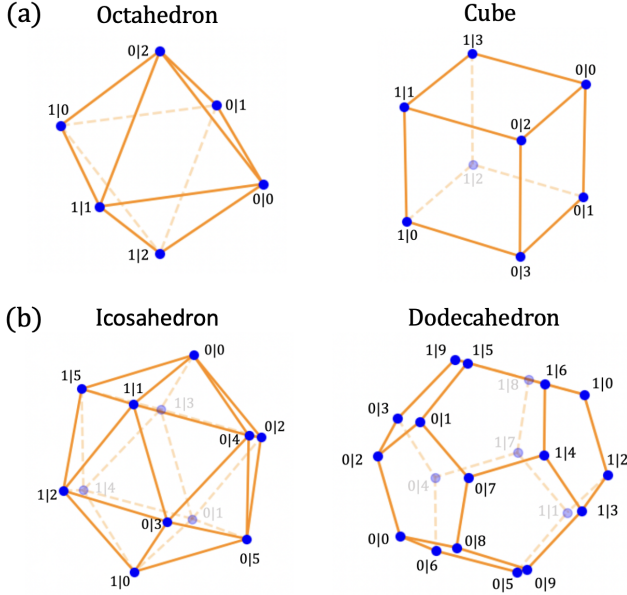


FIG. 5. Geometric configuration of $\mathbf{N} = \{\{N_{a|x}\}_a\}_x$ (Left) and $\mathbf{M} = \{\{M_{b|y}\}_b\}_y$ (Right). (a) Example 2: with cubic and octahedral symmetry; (b) Example 3: with icosahedral and dodecahedral symmetry.

exponentially with the number of measurement settings, making the noncontextual polytope infeasible to fully characterize. Moreover, unlike the standard Bell local polytope, where all vertices are associated to vectors with rational components, the noncontextual polytope generally contains vertices that are associated to vectors with irrational components.

Therefore, instead of fully characterizing the polytope $\mathcal{NC}_{\text{aatt}}$, we employ polytope membership linear programming techniques to derive noncontextuality inequalities. Consider again the scenario with $\Delta_{\mathbf{N}}$ and $\Delta_{\mathbf{M}}$ o -outcome measurements. We can represent the k extreme points $\vec{v} \in \mathcal{NC}_{\text{aatt}} \in \mathbb{R}^d$ as columns of a $d \times k$ matrix $\mathbf{T}_{d,k}$, where $d = o^2 \Delta_{\mathbf{N}} \Delta_{\mathbf{M}}$. A bipartite distribution $p(ab|xy)$, expressed as a probability vector $\vec{p} = \{p_d\}_d := \{p(ab|xy)\}_{abxy}$, lies within the noncontextual polytope if and only if

$$\begin{aligned} & \text{there exists some } x_k \\ & \text{such that } \sum_k \mathbf{T}_{d,k} x_k = p_d, \\ & \text{where } x_k \geq 0_k. \end{aligned} \quad (\text{B3})$$

We can write up the dual of the LP above as:

$$\begin{aligned} & \min_{s_d} \sum_d s_d \cdot p_d \\ & \text{such that } 0_n \leq \sum_d s_d \cdot \mathbf{T}_{d,k} \leq 1_k. \end{aligned} \quad (\text{B4})$$

If there exists a nonclassical correlation $\{p_d\}_d$ that cannot be classically explained, this dual linear program will

always find a real vector $\{s_d\}_d$ satisfying the condition $\sum_d s_d \cdot p_d < 0$. This real vector $\{s_d\}_d$ can then be used to define a facet-defining Bell inequality.

The inequality we gave in Eq. 14 is a facet inequality for the (icosahedron,dodecahedron)-scenario in Example 3. More importantly, for isotropic state ρ_{Iso}^p with $p > \sqrt{\frac{1+\phi^2}{3\phi^4}}$, the inequality can be violated using the following icosahedron and dodecahedron measurements[40, 57]: $M_{a|x} = \frac{1}{2}(\mathbb{1} + (-1)^a \hat{m}_x \cdot \vec{\sigma})$ and $N_{b|y} = \frac{1}{2}(\mathbb{1} + (-1)^b \hat{n}_y \cdot \vec{\sigma})$ with $\hat{m}_x = \frac{1}{\sqrt{1+\phi^2}} \vec{m}_x$ and $\hat{n}_y = \frac{1}{\sqrt{3}} \vec{m}_y$

$$\begin{aligned} \vec{m}_0 &= [0, 1, \phi], \quad \vec{m}_1 = [0, 1, -\phi], \quad \vec{m}_2 = [1, \phi, 0] \\ \vec{m}_3 &= [1, -\phi, 0], \quad \vec{m}_4 = [\phi, 0, 1], \quad \vec{m}_5 = [\phi, 0, -1] \\ \vec{n}_0 &= [-1, -1, -1], \quad \vec{n}_1 = [-\phi, \frac{1}{\phi}, 0], \quad \vec{n}_2 = [-\phi, -\frac{1}{\phi}, 0] \\ \vec{n}_3 &= [-1, -1, 1], \quad \vec{n}_4 = [0, -\phi, \frac{1}{\phi}], \quad \vec{n}_5 = [1, -1, -1] \\ \vec{n}_6 &= [0, -\phi, -\frac{1}{\phi}], \quad \vec{n}_7 = [-1, 1, -1], \quad \vec{n}_8 = [-\frac{1}{\phi}, 0, -\phi] \\ \vec{n}_9 &= [\frac{1}{\phi}, 0, -\phi]. \end{aligned} \quad (\text{B5})$$

Appendix C: Dealing with inexact operational identities

1. Secondary measurements and secondary statistics

Here, we will detail the method of secondary procedures. This method takes as input a set of processes that are obtained by fitting to the relative frequencies and that do not satisfy the required operational identities used in deriving the inequality test, and outputs a set of processes in their convex hull that satisfy these identities exactly.

Consider again a set of measurements on A , $\mathbf{N} = \{\{N_{a|x}\}_a\}_x$, satisfying operational identities $\mathcal{O}_{\text{all}}(\mathbf{N}) = \{\{\alpha_{ax}\}_a\}_x | \sum_{ax} \alpha_{ax} N_{a|x} = 0\}$, describing the ideal identities that one is targeting in the experiment. Any set of operational identities of this form can be reduced to a finite *generating set* [55], meaning that all other operational identities can be deduced from this generating set, and NCOM-realizability relative to this generating set is equivalent to NCOM-realizability relative to the full set. Therefore, we consider only generating sets of operational identities of minimal cardinality. This cardinality, which we denote by $|T|$, coincides with the number of linearly independent operational identities in $\mathcal{O}_{\text{all}}(\mathbf{N})$. A given operational identity can be associated to a vector $\vec{\alpha} = (\alpha_{ax})_{ax}$. Consequently, a minimal generating set can be associated to a set of vectors $\{\vec{\alpha}^{(t)}\}_{t \in T}$. Similar comments apply to the measurements on B .

The procedure for finding the best-fit probabilities to the relative frequencies obtained in the experiment [28,

[46], i.e., the regularization procedure, is detailed in the appendix C2.⁴

As stated in the main text, we refer to the measurements that come out of the regularization procedure as *primary measurements* and denote them by $\mathbf{N}^p = \{\{N_{a|x}^p\}_a\}_x$, and $\mathbf{M}^p = \{\{M_{b|y}^p\}_b\}_y$ respectively.

In general, these measurements do not satisfy the targeted operational identities. Consider the case of the measurements on A . In general $\sum_{ax} \alpha_{ax}^{(t)} N_{a|x}^p \neq 0$ for one or more $\vec{\alpha}^{(t)}$ in a minimal generating set for the targeted set of operational identities, $\mathcal{O}_{\text{all}}(\mathbf{N})$. However, it is possible to find a set of *secondary measurements*, denoted $\mathbf{N}^s = \{\{N_{a|x}^s\}_a\}_x$, such that each of the secondary effects lies in the convex hull of the set of primary effects \mathbf{N}^p , and where the secondary effects exactly satisfy the operational identities $\mathcal{O}_{\text{all}}(\mathbf{N})$, i.e.,

$$\begin{aligned} N_{a|x}^s &= \sum_{a',x'} u_{a',x'}^{a,x} N_{a'|x'}^p \quad \forall a, x \\ \sum_{ax} \alpha_{ax}^{(t)} N_{a|x}^s &= 0 \quad \forall t \in T \\ \sum_{a'x'} u_{a',x'}^{a,x} &= 1, \quad u_{a',x'}^{a,x} \geq 0 \quad \forall a, x, a', x'. \end{aligned} \quad (\text{C1})$$

In particular, we solve an optimization problem that selects the closest approximation to the primary measurements while satisfying these constraints, by maximizing the objective function $C_N = \frac{1}{o\Delta_N} \sum_{a,x} u_{a,x}^{a,x}$, where the value of C_N will be close to 1 when the primary measurements are close to the ideal measurements being targeted. We define the secondary measurements on B , denoted \mathbf{M}^s , similarly. That is, we define $M_{b|y}^s = \sum_{b',y'} v_{b',y'}^{b,y} M_{b'|y'}^p$ and maximize the objective function $C_M = \sum_{b,y} \frac{1}{o\Delta_M} v_{b,y}^{b,y}$ while satisfying the analogues of the constraints in Eq. (C2).

To ensure the existence of a non-trivial set of secondary measurements, the primary measurements must satisfy certain conditions: (1) \mathbf{N}^p should not span a larger operator space than that spanned by the ideal measurements \mathbf{N} , and similarly for \mathbf{M}^p and \mathbf{M} (i.e., the experimental noise does not cause the measurements to drift into a higher-dimensional operator space); and (2) \mathbf{M}^p should be able to prepare steering assemblage on A , i.e., $\{\text{Tr}_B[(\mathbb{1} \otimes M_{b|y}^p) \rho^{AB}]\}_{b,y}$, that spans the same operator space as is spanned by \mathbf{N}^p , and is tomographically complete for the elements of \mathbf{N}^p , and similarly with the roles of \mathbf{N}^p and \mathbf{M}^p reversed.

These two assumptions are significantly milder than those requiring a prior characterization of the measurement devices and can be met in a realistic experiment

when one is confident in the system's dimensionality. Notably, the second assumption allows us to infer the coefficients $u_{a',x'}^{a,x}$ purely from the statistics obtained by the primary measurements, termed the *primary statistics*, using the following linear program:

$$\max \quad C_N = \frac{1}{o\Delta_N} \sum_{ax} u_{ax}^{ax} \quad (\text{C2})$$

$$\begin{aligned} \text{such that} \quad & \sum_{ax|x'} p(a'b'|x'y') u_{a',x'}^{a,x} \alpha_{a,x}^{(t)} = 0 \quad \forall b', y', \forall t \in T \\ & \sum_{aa'x'} p(a'b'|x'y') u_{a',x'}^{a,x} = p(b'|y') \quad \forall b', y'. \\ & \sum_{a'x'} u_{a',x'}^{a,x} = 1, \quad u_{a',x'}^{a,x} \geq 0 \quad \forall a, x, a', x'. \end{aligned}$$

One can obtain the coefficients $v_{b',y'}^{b,y}$ in an analogous fashion.

In the end, the *statistics* defined by the secondary measurements, denoted $p^s(ab|xy)$ and termed the *secondary statistics*, are given by

$$\begin{aligned} p^s(ab|xy) &= \text{Tr}[N_{a|x}^s \otimes M_{b|y}^s \rho^{AB}] \\ &= \sum_{a'b'x'y'} v_{b',y'}^{b,y} u_{a',x'}^{a,x} p(a'b'|x'y'), \end{aligned} \quad (\text{C3})$$

where $p(a'b'|x'y')$ are the statistics defined by the set of primary measurements.

2. Regularization of raw data: frequencies to probabilities

Experiments do not yield probabilities directly. Rather, they yield relative frequencies which under ideal circumstances (of the samples being independent and identically distributed) would converge to the true underlying probabilities in the infinite-run limit. Interpreting relative frequencies as probabilities can lead to a misinterpretation of experimental results. For instance, in a typical Bell experiment, interpreting frequencies as probabilities without accounting for statistical fluctuations can result in an apparent violation of the no-signaling principle [28].

This issue is equally relevant in our experiment. In principle, statistical fluctuations in the relative frequencies could lead to a situation wherein interpreting these as probabilities yields an apparent violation of the predictions of quantum theory (for a given choice of dimensionality of systems). To address this issue, we adapted a well-motivated regularization method, similar to those used in previous works [26, 28, 46], to convert the experimentally observed relative frequencies into *estimates* of the true distribution. Specifically, we denote the frequency obtained directly from raw data in a bipartite scenario as $f(ab|xy)$ and its variance as $\Delta f(ab|xy)$. We

⁴ We note that the procedure relies on an assumption about the dimension of the quantum (or GPT) system, although one can also do the fit in a way that *infers* the optimal GPT dimension from the experimental data using a train-and-test methodology rather than assuming it a priori [26, 50].

then consider the weighted χ^2 optimization, where

$$\chi^2 := \min_{p(ab|xy)} \sum_{abxy} \left| \frac{f(ab|xy) - p(ab|xy)}{\Delta f(ab|xy)} \right|^2. \quad (\text{C4})$$

(Note that one could also replace the χ^2 function with the L^2 function or the KL divergence, as discussed in [28].) In our data analysis, we considered two types of theoretical models to fit the relative frequencies. The first assumes quantum mechanics with a fixed Hilbert space dimension D (hence, operator space dimension D^2), where $p(ab|xy) = \text{tr}[(N_{a|x} \otimes M_{b|y})\rho^{AB}]$. The second allows for a realization in an arbitrary generalized probabilistic theory (GPT) with fixed GPT vector space dimension D^2 , where $p(ab|xy) = n_{a|x} \otimes m_{b|y} \cdot G^{AB}$. In this case, $n_{a|x}$, $m_{b|y}$, and G^{AB} are GPT vectors corresponding to unipartite effects on A and B and the bipartite state on AB respectively.

As the two regularization methods yielded no statistically significant differences, we used the quantum realization. We note that the associated optimization problem cannot be solved in a single step; instead, we employ a see-saw algorithm to iteratively optimize the bipartite state and local effects, i.e.,

1. Given an initial guess for \mathbf{N} , \mathbf{M} and ρ^{AB} ,
2. Fix \mathbf{N} and \mathbf{M} and update states ρ^{AB} to be $\text{argmin}_{\rho^{AB}} \sum_{abxy} \left| \frac{f(ab|xy) - \text{Tr}[(N_{a|x} \otimes M_{b|y})\rho^{AB}]}{\Delta f(ab|xy)} \right|^2$,
3. Fix \mathbf{N} and state ρ^{AB} , and update \mathbf{M} to be $\text{argmin}_{\mathbf{M}} \sum_{abxy} \left| \frac{f(ab|xy) - \text{Tr}[(N_{a|x} \otimes M_{b|y})\rho^{AB}]}{\Delta f(ab|xy)} \right|^2$,
4. Fix \mathbf{M} and state ρ^{AB} , and update \mathbf{N} to be $\text{argmin}_{\mathbf{N}} \sum_{abxy} \left| \frac{f(ab|xy) - \text{Tr}[(N_{a|x} \otimes M_{b|y})\rho^{AB}]}{\Delta f(ab|xy)} \right|^2$,
5. Repeat step 2-4 until it converges relative to a certain threshold.

Each step of the optimization above can be expressed as a quadratic program, which could be efficiently solved computationally. However, since the bipartite statistics $p(ab|xy)$ are invariant under invertible local transformations (the tomographic gauge freedom noted in Ref. [27] and described in the main text) the optimization does not yield a unique solution for the bipartite state ρ^{AB} and the sets of local effects \mathbf{N} and \mathbf{M} .

These regularization procedures are closely related to GPT tomography [26] and gate-set tomography [27]. Consequently, any tools developed for such bootstrap tomography schemes can be directly applied here as well. However, we do not use this scheme in the conventional manner that it would be used to achieve entanglement certification, namely, by implementing a separability test on the bipartite state that is the output of the tomography scheme. We avoid this approach because this output is gauge-dependent and would require an optimization

over the choice of gauge. Instead, our entanglement certification technique evaluates noncontextuality inequalities on the regularized statistics, and since these are gauge-independent quantities, no optimization over gauge is required.

Furthermore, since the characterization of the bipartite state is not our objective, a distinct but equivalent approach can be taken to regularize the raw statistics. Specifically, rather than employing a see-saw algorithm to iteratively optimize the bipartite state on AB and the sets of local effects on A and on B , one can instead just iteratively optimize the steering assemblage on A , $\{\{\tilde{\rho}_{b|y}\}\}_{b,y}$, where $\tilde{\rho}_{b|y} = \text{Tr}_B[(1 \otimes M_{b|y})\rho^{AB}]$ and the set of local effects on A , \mathbf{N} (or, equivalently, the steering assemblage and set of local effects on B). The GPT version of this regularization process is precisely the one studied in the prepare-and-measure scenario in [26].

It is worth noting again that because of the tomographic gauge freedom described in the main text, there is a nonuniqueness in the output of the fitting procedure that yields the bipartite state and the primary measurements, and hence a nonuniqueness in the secondary measurements as well. However, the secondary statistics (like the primary statistics) are manifestly gauge-independent. Because it is the secondary statistics on which the noncontextuality inequalities are tested, such tests in our protocol are gauge-independent.

Appendix D: Experimental details

1. Generating isotropic states experimentally

We generate polarization-entangled photons using type-II spontaneous parametric down-conversion inside a Sagnac interferometer consisting of a 404 nm continuous-wave (cw) diode laser and a 10mm PPKTP crystal. The source aims to generate the Bell state $|\Phi^+\rangle = \frac{1}{\sqrt{2}}(|HH\rangle + |VV\rangle)$, and is implemented with measured state fidelity greater than 97.5% at a rate of 40000 coincidences/second for a laser power of 4 mW. The photons are then sent through a depolarization channel composed of two liquid crystal retarders (LCR) which depolarize the maximally entangled state to a high-fidelity isotropic state by producing a probabilistic mixture of Bell states as in Table III.

TABLE III. Isotropic state generation

Gate	Probability	Output
$\hat{1} \otimes \hat{1}\hat{1}$	$p^{\text{set}} + \frac{1-p^{\text{set}}}{4}$	$ \Phi^+\rangle = HH\rangle + VV\rangle$
$\hat{1} \otimes \hat{1}\hat{Z}$	$\frac{1-p^{\text{set}}}{4}$	$ \Phi^-\rangle = HH\rangle - VV\rangle$
$\hat{1} \otimes \hat{X}\hat{1}$	$\frac{1-p^{\text{set}}}{4}$	$ \Psi^+\rangle = HV\rangle + VH\rangle$
$\hat{1} \otimes \hat{X}\hat{Z}$	$\frac{1-p^{\text{set}}}{4}$	$ \Psi^-\rangle = HV\rangle - VH\rangle$

The produced isotropic state typically has a value of the parameter p that deviates slightly from the value p^{set}

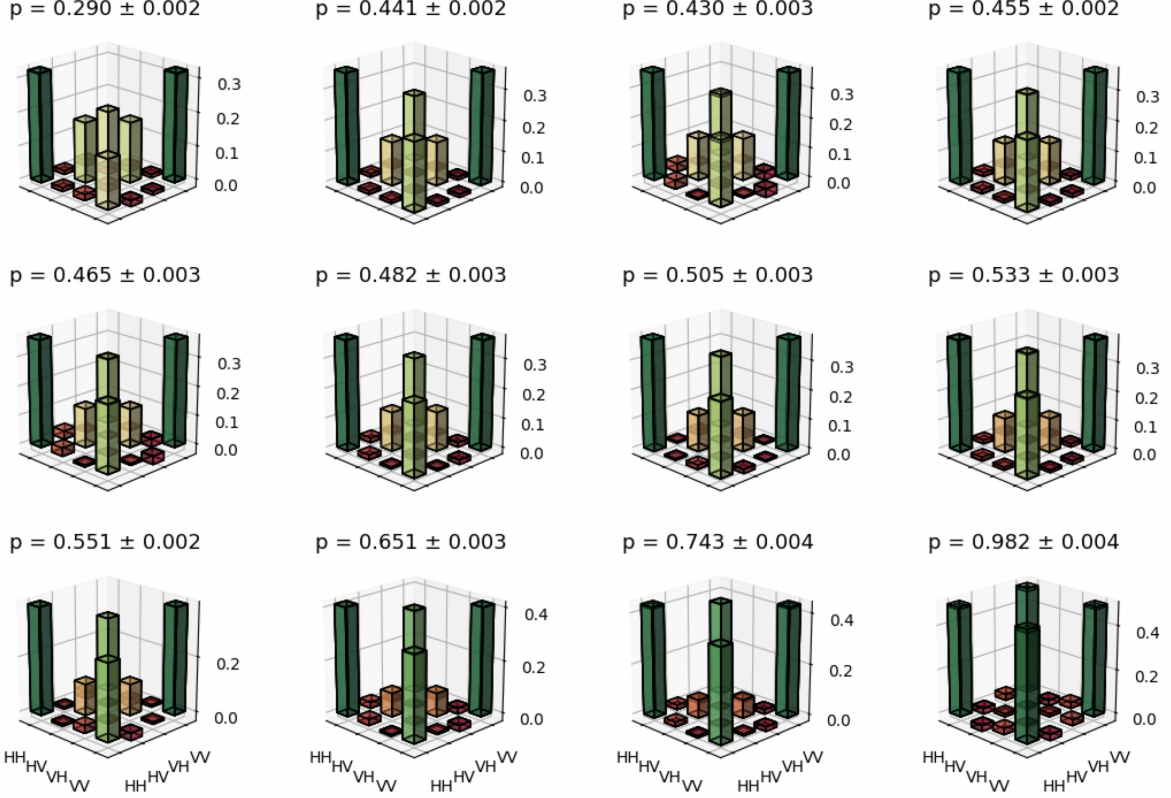


FIG. 6. Quantum state tomography results: the real part of the reconstructed density matrix is shown, while the imaginary components are negligible, with values below 0.02. The parameter p denotes the weight of the closest isotropic state, with error bars estimated from 100 Monte Carlo trials accounting for both statistical and systematic uncertainties (see text below).

that was targeted due to the initial state's non-unit fidelity with $|\Phi^+\rangle$ and the LCR's limited switching speed (80 ms hold time per setting, with 5 ms rise time and 20 ms fall time). Instead of relying solely on the targeted value p^{set} , we estimated the realized value using the measured fidelity to the nearest isotropic state. In table IV, we compare the targeted and estimated values, showing that the fidelity between the tomographically reconstructed state and the nearest isotropic state is consistently above 99%.

2. Measurement technique

After preparing each isotropic state, we record coincidence events from both the transmitted and reflected output ports using single-photon avalanche diodes (SPCM-AQRH-11-FC, Excelitas) with a 1 ns coincidence window, and a 5 s measurement time per measurement configuration. We measure coincidence counts of the two photons in measurement configurations corresponding to the vertices of the shapes associated to the set of measurements being targeted. It is important to note that the polarizing beam splitters have different efficiencies for their transmitted and reflected ports, which has the potential

to add non-isotropic noise to our state. To mitigate this noise, we follow the measurement scheme outlined in Table V, where instead of assigning specific ports to specific effects, we iterate over the four permutations of ports and effects by adjusting the wave plates accordingly. Next, for each effect, we take the four trials (one per port configuration) and sum the coincidence counts for the desired effect. Finally, we divide each coincident by the sum of the four to convert counts into relative frequencies for one measurement configuration. In total, 240 distinct measurement configurations are implemented in the same way, resulting in a total integration time of approximately 2 hours. These raw relative frequencies are then converted to the raw frequency corresponding to the 60 measurement settings (effectively each setting is measured in four different experimental configurations).

3. Experimental error analysis

The experimental uncertainty in the noncontextual bound \mathcal{I} is estimated using a Monte Carlo simulation with 100 independent trials, where each trial samples from a Poisson distribution based on the observed raw counts. To further quantify the uncertainties in the esti-

p^{set}	$\mathcal{F}(\rho_{\text{iso}}^{p^{\text{set}}}, \rho^{\text{tomo}})$	p	$\mathcal{F}(\rho_{\text{iso}}^p, \rho^{\text{tomo}})$	\mathcal{I}
0.270	0.9949 \pm 0.0007	0.290 \pm 0.002	0.9950 \pm 0.0006	0.04513 \pm 0.00015
0.420	0.9965 \pm 0.0009	0.441 \pm 0.002	0.9967 \pm 0.0009	0.00578 \pm 0.00021
0.430	0.9892 \pm 0.0010	0.430 \pm 0.003	0.9892 \pm 0.0010	0.01068 \pm 0.00019
0.440	0.9966 \pm 0.0008	0.454 \pm 0.002	0.9963 \pm 0.0008	-0.00117 \pm 0.00022
0.450	0.9934 \pm 0.0011	0.465 \pm 0.002	0.9936 \pm 0.0011	-0.00409 \pm 0.00018
0.480	0.9938 \pm 0.0012	0.483 \pm 0.003	0.9938 \pm 0.0012	-0.00585 \pm 0.00039
0.500	0.9962 \pm 0.0011	0.505 \pm 0.003	0.9962 \pm 0.0011	-0.01207 \pm 0.00018
0.520	0.9935 \pm 0.0013	0.534 \pm 0.003	0.9936 \pm 0.0013	-0.01633 \pm 0.00016
0.540	0.9957 \pm 0.0010	0.551 \pm 0.002	0.9958 \pm 0.0010	-0.02583 \pm 0.00022
0.650	0.9911 \pm 0.0017	0.651 \pm 0.003	0.9911 \pm 0.0017	-0.05280 \pm 0.00011
0.750	0.9869 \pm 0.0029	0.742 \pm 0.004	0.9870 \pm 0.0030	-0.07849 \pm 0.00012
1.000	0.9689 \pm 0.0036	0.982 \pm 0.004	0.9802 \pm 0.0043	-0.14256 \pm 0.00013

TABLE IV. Experimental results for 12 tomographically reconstructed quantum states for which the parameter value being targeted is p^{set} and the parameter of the closest isotropic state is p . In red: Unsteerable states that violate the inequality $\mathcal{I} \geq 0$ in the main text; In yellow: States that violate the inequality in the main text but for which the entanglement could in principle be certified by violation of a steering inequality. The uncertainties in the violations arise from Poissonian statistics, whereas the uncertainties in p and in fidelities are calculated from Monte Carlo simulations of the different state tomography results, as described in the text.

TABLE V. Measurement iteration scheme for setting xy

Iter#	Alice Trans.	Alice Refl.	Bob Trans.	Bob Refl.
1	$N_{0 x}$	$N_{1 x}$	$M_{0 y}$	$M_{1 y}$
2	$N_{1 x}$	$N_{0 x}$	$M_{1 y}$	$M_{0 y}$
3	$N_{0 x}$	$N_{1 x}$	$M_{1 y}$	$M_{0 y}$
4	$N_{1 x}$	$N_{0 x}$	$M_{0 y}$	$M_{1 y}$

imated state parameter p and to certify the unsteerability of the states, we also account for systematic errors in the wave plate settings by drawing these from a normal distribution, similarly as reported in Ref. [58].

Specifically, we consider two primary sources of systematic error: (1) miscalibration or model imperfection of the measurement wave plates, modeled as a Gaussian distribution over phase shifts with a standard deviation of 1° , and (2) phase shifts introduced by model imperfections also assumed to have an uncertainty of 1° . For each trial, the reconstructed density matrix is used to estimate the isotropic state parameter p , and the standard deviation across all trials is reported as the final uncertainty. Additional details and data are summarized in the Appendix D.

4. Detailed Experimental Results

The validity of our experimental outcomes—and the subsequent violation of the inequality under study—is inherently linked to the precision of our isotropic state preparation. Recall that the fidelity \mathcal{F} between states ρ and σ is defined as follows:

$$\mathcal{F}(\rho, \sigma) = \text{Tr} \left(\sqrt{\sqrt{\rho} \sigma \sqrt{\rho}} \right)^2. \quad (\text{D1})$$

While the main text highlights a fidelity between our realized state and the best-matched isotropic state that

TABLE VI. C_N and C_M value for different experiment data.

p	C_M	C_N
0.290	0.959	0.937
0.442	0.958	0.980
0.430	0.946	0.972
0.453	0.950	0.982
0.465	0.960	0.982
0.483	0.955	0.957
0.506	0.956	0.969
0.534	0.956	0.972
0.551	0.959	0.971
0.650	0.966	0.981
0.741	0.972	0.985
0.992	0.970	0.985

TABLE VII. Experimental results on optimal secondary measurements: For each quantum state involved in the test, we report the optimal values of the parameters C_N and C_M obtained during the construction of the secondary measurements.

exceeds 99%, this section provides a detailed evaluation of our measured fidelity with respect to both the best-matched isotropic state and the state we targeted. To rigorously assess the quality of our state preparation, we performed quantum state tomography using the same experimental setup described earlier. Measurements were conducted across all 12×20 basis settings, with the corresponding Bloch vectors arranged to realize the geometries of the icosahedron and dodecahedron, and the quantum state tomography is done by minimizing the L^2 norm

$$L^2 = |P_i - \langle \psi_i | \rho | \psi_i \rangle|^2, \quad (\text{D2})$$

where $|\psi_i\rangle$ represents the i^{th} measurement setting, and P_i is the corresponding relative frequency. The result of this optimization yields a density operator, which is denoted ρ^{tomo} .

To address potential mischaracterizations of ρ^{tomo} due

to statistical and systematic errors, we conducted a comprehensive Monte Carlo simulation comprising 100 trials. In this simulation: (1) Raw count data were modeled using Poissonian statistics; (2) The calibration of the measurement wave-plate angles was simulated using a normal distribution over phase-shifts with a standard deviation of 1° ; (3) Variations in wave-plate thickness—leading to phase-shift errors—were also represented by a normal distribution with 1° of phase shift error.

After reconstructing the density operator via tomography, we computed its fidelity with the target isotropic state (defined by parameter p^{set}), and the closest isotropic state (defined by parameter p).

The results, summarized in Table IV, confirm that for each of the 12 values of p^{set} we considered, our realized state had a fidelity with our targeted state and a fidelity with the best-matched isotropic state of approximately 99%.

Appendix E: Certifying unsteerability for states

In our experiment, the prepared state is never exactly an isotropic state (for which unsteerability and locality are well-studied [6, 8]). Therefore, in addition to noting the high fidelity of the states we prepare with an unsteerable state, we provide a direct demonstration of the unsteerability of some of the states we realized in the experiment.

To achieve this, we employ recent findings in Ref. [43, 44], which show that the isotropic state $\rho_{\text{Iso}}^p = p|\Phi^+\rangle\langle\Phi^+| + (1-p)\frac{1\otimes 1}{8}$ is unsteerable for $p \leq \frac{1}{2}$. We make use of each of the following facts:

(1) any state $\rho = (\mathbb{1} \otimes U)\rho_{\text{Iso}}^p(\mathbb{1} \otimes U^\dagger)$ where $p \leq \frac{1}{2}$ re-

mains unsteerable for any unitary U ;

- (2) all separable states are unsteerable;
- (3) any convex combination of unsteerable states is unsteerable,

We can witness the unsteerability of our realized state ρ if we find feasible solutions of the following semidefinite program:

$$X \succeq 0, \quad X^{T_B} \succeq 0, \quad p_i \geq 0 \quad \forall i, \\ \sum_{i=1}^n p_i \rho_i + X = \rho,$$

where $\rho_i = (\mathbb{1} \otimes U_i)\rho_{\text{Iso}}^p(\mathbb{1} \otimes U_i^\dagger)$ where $p \leq 1/2$ for some U_i sampled from the Haar measure of $SU(2)$ and X is any two-qubit quantum state with a positive partial transpose (and so is separable). That is, feasibility of this program is a sufficient condition for unsteerability.

Moreover, following an argument similar to that in Ref. [58], the fact (1) can be replaced with a more general statement for any positive map; that is, any state $\rho = (\mathbb{1} \otimes \Lambda)(\rho_{\text{Iso}}^p) \geq 0$ where $p \leq 1/2$ remains unsteerable for any positive map Λ [58]. Using this condition leads to a slightly different SDP that is generally capable of certifying a broader class of unsteerable states.

The numerics show that two of the states we realized in our experiment, those with estimated isotropic parameters $p = 0.454$ and $p = 0.465$, yield feasible solutions to the SDP (even after Monte Carlo simulations accounting for small measurement imperfections), thereby confirming their unsteerability. However, the state with estimated isotropic parameter $p = 0.483$ fails this test and thus cannot be concluded to be unsteerable even though it is known to be close to an unsteerable isotropic state.

[1] J. S. Bell, On the Einstein Podolsky Rosen paradox, *Physics Physique Fizika* **1**, 195 (1964).

[2] C. J. Wood and R. W. Spekkens, The lesson of causal discovery algorithms for quantum correlations: causal explanations of Bell-inequality violations require fine-tuning, *New Journal of Physics* **17**, 033002 (2015).

[3] N. Brunner, D. Cavalcanti, S. Pironio, V. Scarani, and S. Wehner, Bell nonlocality, *Rev. Mod. Phys.* **86**, 419 (2014).

[4] R. Horodecki, P. Horodecki, M. Horodecki, and K. Horodecki, Quantum entanglement, *Rev. Mod. Phys.* **81**, 865 (2009).

[5] R. Uola, A. C. S. Costa, H. C. Nguyen, and O. Gühne, Quantum steering, *Rev. Mod. Phys.* **92**, 015001 (2020).

[6] R. F. Werner, Quantum states with Einstein-Podolsky-Rosen correlations admitting a hidden-variable model, *Phys. Rev. A* **40**, 4277 (1989).

[7] M. Piani, S. Gharibian, G. Adesso, J. Calsamiglia, P. Horodecki, and A. Winter, All nonclassical correlations can be activated into distillable entanglement, *Phys. Rev. Lett.* **106**, 220403 (2011).

[8] H. M. Wiseman, S. J. Jones, and A. C. Doherty, Steering, entanglement, nonlocality, and the Einstein-Podolsky-Rosen paradox, *Phys. Rev. Lett.* **98**, 140402 (2007).

[9] D. Schmid, T. C. Fraser, R. Kunjwal, A. B. Sainz, E. Wolfe, and R. W. Spekkens, Understanding the interplay of entanglement and nonlocality: motivating and developing a new branch of entanglement theory, *Quantum* **7**, 1194 (2023).

[10] M. T. Quintino, T. Vértesi, D. Cavalcanti, R. Augusiak, M. Demianowicz, A. Acín, and N. Brunner, Inequivalence of entanglement, steering, and Bell nonlocality for general measurements, *Phys. Rev. A* **92**, 032107 (2015).

[11] Bell's inequality holds for all non-product states, *Physics Letters A* **154**, 201 (1991).

[12] N. Gisin and A. Peres, Maximal violation of Bell's inequality for arbitrarily large spin, *Physics Letters A* **162**, 15 (1992).

[13] J. Barrett, Nonsequential positive-operator-valued measurements on entangled mixed states do not always violate a Bell inequality, *Phys. Rev. A* **65**, 042302 (2002).

[14] J. F. Clauser, M. A. Horne, A. Shimony, and R. A. Holt, Proposed experiment to test local hidden-variable theories, *Phys. Rev. Lett.* **23**, 880 (1969).

[15] O. Ghne and G. Tth, Entanglement detection, *Physics Reports* **474**, 1 (2009).

[16] C. Branciard, D. Rosset, Y.-C. Liang, and N. Gisin, Measurement-device-independent entanglement witnesses for all entangled quantum states, *Phys. Rev. Lett.* **110**, 060405 (2013).

[17] F. Buscemi, All entangled quantum states are nonlocal, *Phys. Rev. Lett.* **108**, 200401 (2012).

[18] R. W. Spekkens, Contextuality for preparations, transformations, and unsharp measurements, *Phys. Rev. A* **71**, 052108 (2005).

[19] S. Kochen and E. P. Specker, The problem of hidden variables in quantum mechanics, in *The Logico-Algebraic Approach to Quantum Mechanics: Volume I: Historical Evolution*, edited by C. A. Hooker (Springer Netherlands, Dordrecht, 1975) pp. 293–328.

[20] C. Budroni, A. Cabello, O. Ghne, M. Kleinmann, and J.-A. Larsson, Kochen-specker contextuality, *Rev. Mod. Phys.* **94**, 045007 (2022).

[21] D. Schmid, J. H. Selby, and R. W. Spekkens, Addressing some common objections to generalized noncontextuality, *Phys. Rev. A* **109**, 022228 (2024).

[22] R. W. Spekkens, Negativity and contextuality are equivalent notions of nonclassicality, *Phys. Rev. Lett.* **101**, 020401 (2008).

[23] D. Schmid, J. H. Selby, M. F. Pusey, and R. W. Spekkens, A structure theorem for generalized-noncontextual ontological models, *Quantum* **8**, 1283 (2024).

[24] D. Schmid, J. H. Selby, E. Wolfe, R. Kunjwal, and R. W. Spekkens, Characterization of noncontextuality in the framework of generalized probabilistic theories, *PRX Quantum* **2**, 010331 (2021).

[25] F. Shahandeh, Contextuality of general probabilistic theories, *PRX Quantum* **2**, 010330 (2021).

[26] M. D. Mazurek, M. F. Pusey, K. J. Resch, and R. W. Spekkens, Experimentally bounding deviations from quantum theory in the landscape of generalized probabilistic theories, *PRX Quantum* **2**, 020302 (2021).

[27] E. Nielsen, J. K. Gamble, K. Rudinger, T. Scholten, K. Young, and R. Blume-Kohout, Gate Set Tomography, *Quantum* **5**, 557 (2021).

[28] P.-S. Lin, D. Rosset, Y. Zhang, J.-D. Bancal, and Y.-C. Liang, Device-independent point estimation from finite data and its application to device-independent property estimation, *Phys. Rev. A* **97**, 032309 (2018).

[29] J. Bowles, I. Šupi, D. Cavalcanti, and A. Acn, Device-independent entanglement certification of all entangled states, *Phys. Rev. Lett.* **121**, 180503 (2018).

[30] A. Tavakoli and R. Uola, Measurement incompatibility and steering are necessary and sufficient for operational contextuality, *Phys. Rev. Res.* **2**, 013011 (2020).

[31] V. J. Wright and M. Farkas, Invertible map between Bell nonlocal and contextuality scenarios, *Phys. Rev. Lett.* **131**, 220202 (2023).

[32] M. Plvala and O. Ghne, Contextuality as a precondition for quantum entanglement, *Phys. Rev. Lett.* **132**, 100201 (2024).

[33] T. Proctor, K. Rudinger, K. Young, M. Sarovar, and R. Blume-Kohout, What randomized benchmarking actually measures, *Phys. Rev. Lett.* **119**, 130502 (2017).

[34] G. Chiribella, G. M. D'Ariano, and P. Perinotti, Probabilistic theories with purification, *Phys. Rev. A* **81**, 062348 (2010).

[35] Y. Zhang, D. Schmid, Y. Ying, and R. W. Spekkens, Reassessing the boundary between classical and nonclassical for individual quantum processes, arXiv preprint arXiv:2503.05884 (2025).

[36] P. Skrzypczyk, M. Navascus, and D. Cavalcanti, Quantifying Einstein-Podolsky-Rosen steering, *Phys. Rev. Lett.* **112**, 180404 (2014).

[37] D. Rosset, D. Schmid, and F. Buscemi, Type-independent characterization of spacelike separated resources, *Phys. Rev. Lett.* **125**, 210402 (2020).

[38] Y. Zhang, Y. Ying, and D. Schmid, Quantifiers and witnesses for the nonclassicality of measurements and of states, arXiv preprint arXiv:2504.02944 (2025).

[39] The Royal Swedish Academy of Sciences, Scientific Background on the Nobel Prize in Physics 2022: Experiments with Entangled Photons, Establishing the Violation of Bell Inequalities and Pioneering Quantum Information Science, <https://www.nobelprize.org/uploads/2022/10/advanced-physicsprize2022.pdf> (2022), [Accessed: November 5, 2024].

[40] D. J. Saunders, S. J. Jones, H. M. Wiseman, and G. J. Pryde, Experimental EPR-steering using Bell-local states, *Nature Physics* **6**, 845 (2010).

[41] S. Designolle, G. Iommazzo, M. Besanon, S. Knebel, P. Gel, and S. Pokutta, Improved local models and new Bell inequalities via frank-wolfe algorithms, *Phys. Rev. Res.* **5**, 043059 (2023).

[42] A. Acn, N. Gisin, and B. Toner, Grothendieck's constant and local models for noisy entangled quantum states, *Phys. Rev. A* **73**, 062105 (2006).

[43] Y. Zhang and E. Chitambar, Exact steering bound for two-qubit werner states, *Phys. Rev. Lett.* **132**, 250201 (2024).

[44] M. J. Renner, Compatibility of generalized noisy qubit measurements, *Phys. Rev. Lett.* **132**, 250202 (2024).

[45] T. Kim, M. Fiorentino, and F. N. C. Wong, Phase-stable source of polarization-entangled photons using a polarization sagnac interferometer, *Phys. Rev. A* **73**, 012316 (2006).

[46] M. D. Mazurek, M. F. Pusey, R. Kunjwal, K. J. Resch, and R. W. Spekkens, An experimental test of noncontextuality without unphysical idealizations, *Nature Communications* **7**, ncomms11780 (2016).

[47] L. Hardy, Quantum theory from five reasonable axioms (2001), arXiv:quant-ph/0101012 [quant-ph].

[48] J. Barrett, Information processing in generalized probabilistic theories, *Phys. Rev. A* **75**, 032304 (2007).

[49] M. Krystek and M. Anton, A weighted total least-squares algorithm for fitting a straight line, *Measurement Science and Technology* **18**, 3438 (2007).

[50] M. J. Graboweczyk, C. A. J. Pollack, A. R. Cameron, R. W. Spekkens, and K. J. Resch, Experimentally bounding deviations from quantum theory for a photonic three-level system using theory-agnostic tomography, *Phys. Rev. A* **105**, 032204 (2022).

[51] M. F. Pusey, L. del Rio, and B. Meyer, Contextuality without access to a tomographically complete set (2019), arXiv:1904.08699 [quant-ph].

[52] D. Schmid, J. H. Selby, V. P. Rossi, R. D. Baldijo, and A. B. Sainz, Shadows and subsystems of generalized probabilistic theories: when tomographic incompleteness is not a loophole for contextuality proofs (2024), arXiv:2409.13024 [quant-ph].

[53] Y. Zhang, Bipartite-nonclassicality: Data and code (2025), GitHub repository. Commit 1932f03, accessed 12,

Apr,2025.

[54] P. Busch, Quantum states and generalized observables: A simple proof of gleason's theorem, *Phys. Rev. Lett.* **91**, 120403 (2003).

[55] D. Schmid, R. D. Baldijão, J. H. Selby, A. B. Sainz, and R. W. Spekkens, Noncontextuality inequalities for prepare-transform-measure scenarios, *arXiv preprint* (2024), [arXiv:2407.09624 \[quant-ph\]](https://arxiv.org/abs/2407.09624).

[56] D. Schmid, R. W. Spekkens, and E. Wolfe, All the noncontextuality inequalities for arbitrary prepare-and-measure experiments with respect to any fixed set of operational equivalences, *Phys. Rev. A* **97**, 062103 (2018).

[57] Y. Zhang, J. Zhang, and E. Chitambar, Cost of simulating entanglement in steering scenario, *arXiv e-prints* , arXiv (2023).

[58] L. Villegas-Aguilar, E. Polino, F. Ghafari, M. T. Quintino, K. T. Laverick, I. R. Berkman, S. Rogge, L. K. Shalm, N. Tischler, E. G. Cavalcanti, S. Slussarenko, and G. J. Pryde, Nonlocality activation in a photonic quantum network, *Nature Communications* **15**, 3112 (2024).